

Petrology and geochronology of “muscovite age standard” B4M

Alexandra R. Heri^{1,2}, Martin Robyr¹, Igor M. Villa^{1,3}

1 - Institut für Geologie, Universität Bern, 3012 Bern, Switzerland; heri.alexandra@gmail.com

2 - Department of Earth Sciences, The University of Hong Kong, Pokfulam Road, Hong Kong

3 - Dipartimento di Scienze Geologiche e Geotecnologie, Università di Milano Bicocca, 20126 Milano, Italy

Abstract

Muscovite B4M, distributed in 1961 as an age standard, was ground under ethanol. Five grain size fractions were obtained and characterised by X-ray diffraction. They display a mixing trend between a phengitic (enriched in the fraction $< 0.2 \mu\text{m}$) and a muscovitic component (predominant in the fraction $> 20 \mu\text{m}$). High-pressure phengite is preserved as a relict in retrograde muscovite.

Electron microprobe analyses on the distributed mineral separate reveal at least four white mica populations based on Si, Al, Mg, Na, Fe, and F. Rb/K ratios vary by one order of magnitude. Rb-Sr analyses link the mineralogical heterogeneity to variable Rb/Sr and $^{87}\text{Sr}/^{86}\text{Sr}$ ratios. The grain size fractions define no internal isochron. Relict fine-grained phengite gives older ages than coarse-grained retrograde greenschist facies muscovite.

The inverse grain size - age relationship also characterises ^{39}Ar - ^{40}Ar analyses. Cl/K anticorrelates with step ages: Cl-rich coarse muscovite is younger than Cl-poor fine relict phengite. Sr and Ar preserve a similar isotopic inheritance despite peak metamorphism reaching $635 \pm 20 \text{ }^\circ\text{C}$.

A suitable mineral standard requires that especially its petrological equilibrium first be demonstrated. Relicts and retrograde reaction textures are a guarantee of isotopic disequilibrium and heterogeneous ages within single crystal at the μm scale.

Key words: age standard, geochronology, petrological disequilibrium, isotopic inheritance, white mica retentivity

29

Introduction

30

31 Following the metrological definition, “a standard is a realisation of the definition of a given
32 quantity” (VIM 2008, entry 5.1); it can consist of a reference material, which by definition must be
33 sufficiently homogeneous to be fit for its intended use in measurement (VIM 2008, entry 5.13). In
34 the Earth Sciences, one essential problem that limits the correct uncertainty assessment of the
35 measurements is the extent to which natural samples can be traced to reference materials that, in
36 turn, can be traced to primary standards that embody the SI units. It is frequently assumed that there
37 exist natural geological samples that fulfill the requirements of metrological suitability completely.
38 A general discussion of this assumption is beyond the scope of this paper. What will be addressed
39 here is a case study on one “standard” (actually at best a “reference material”) previously described
40 as suitable to calibrate the Rb-Sr and K-Ar isotopic dating systems.

41 The B4M muscovite was first analysed by Jäger and Faul (1959). The sampling locality is given by
42 Jäger *et al.* (1963) as “Togni quarry, Brione” (Central Alps). The metamorphic conditions were $T =$
43 635 ± 20 °C, $p = 6.3 \pm 0.3$ kbar (Todd and Engi 1997; Engi, personal communication 2011). While
44 a gneiss sample from the same quarry in Brione does exist in the teaching collection of the
45 University of Bern, our results (see below) suggest that it is not from the same rock used for the
46 preparation of the B4M muscovite separate.

47 The Rb-Sr age of B4M, 16 ± 20 Ma, was calculated by Jäger (1962, her Table 1) by assuming an
48 initial Sr isotopic composition equal to present-day ocean water. The muscovite was subsequently
49 separated in large amounts and distributed to geochronology laboratories world-wide, with a stated
50 nominal grain size of 35-50 mesh, or 300-500 μm . The K-Ar ages obtained by numerous
51 laboratories in a round-robin experiment using the distributed separate, were compiled by Flisch
52 (1982), who concluded by proposing a preferred K-Ar age of 18.6 ± 0.2 Ma.

53 The assumption underlying the use of a polymetamorphic mineral as a natural standard was the very
54 same of Jäger’s (1967) thermochronological approach: because the gneiss had undergone

55 metamorphic temperatures in excess of 600 °C, assuming that muscovites record “cooling” below
56 350 °C (or 400 °C, or 450 °C, as subsequent workers attempted to correct), then all muscovite
57 grains record post-metamorphic cooling, and hence fulfill the requirement of homogeneity. Later
58 work by Dodson (1986) apparently introduces some complication, as each grain that underwent
59 diffusive ^{40}Ar and ^{87}Sr loss would record a concentric ^{40}Ar and ^{87}Sr gradient; grinding the rock and
60 breaking up grains would generate an artificial heterogeneity by producing subgrains consisting of
61 ^{40}Ar - ^{87}Sr -poor rims and others of ^{40}Ar - ^{87}Sr -rich cores. However, the petrographic description by
62 Jäger *et al.* (1963) states that the grain size of major minerals of the gneiss is 0.5-2 mm. This
63 ensures that most grains of the distributed B4M separate are not minute fragments, and thus that
64 they are “sufficiently” homogeneous in the original assumption of a single mica population that
65 records at most Ar and Sr diffusion out of coherent large grains.

66

67

68

Analytical techniques

69

70 Grinding and size separation: ca. 1 g of the 300-500 μm B4M grains were ground for 4 hours in an
71 agate mill under ethanol. This artificial sample was then suspended in Atterberg cylinders in
72 distilled water and separated into five grain sizes ($> 20 \mu\text{m}$, 6-20 μm , 2-6 μm , 0.6-2 μm , $< 0.6 \mu\text{m}$),
73 labelled A (finest) to E (coarsest).

74 Rb-Sr isotope analyses: The five grain size fractions A-E were dried after settling, spiked with a
75 mixed ^{84}Sr + ^{87}Rb spike, then exposed to hot aqua regia for 24 h. This is sufficient to entirely
76 solubilise the interlayer cations (Villa *et al.* 2006). Rb and Sr were separated on cation resin
77 columns and analysed on a NuInstruments™ multicollector plasma-source mass spectrometer,
78 following the protocol in Villa *et al.* (2006).

79 X-Ray Diffraction: The analyses of samples A-E were performed with a Philips PW1800 using Cu
80 $K\alpha$ radiation ($\lambda = 1.54598 \text{ \AA}$), an acceleration voltage of 40 kV and an electron generating current
81 of 30 mA. The measurement step size was 0.02° and the scan speed 2 s/step.

82 Electron microprobe: A few hundred grains of the distributed separate were mounted in two
83 different orientations: one by laying grains (subsequently labelled ‘flat’) parallel to the polishing
84 surface, resting on the {001} plane, and one arranging grains (labelled ‘vert’) perpendicular to the
85 polishing surface, exposing the interlayers. Both mounts were gently polished, carbon-coated and
86 analysed with a JEOL™ 8200 electron microprobe (EMP) at the Institut für Geologie, Universität
87 Bern. Wavelength-dispersive analyses were performed with a beam diameter of ca. 5 μm , an
88 accelerating potential of 15 kV and a beam current of 15 nA.

89 ^{39}Ar - ^{40}Ar stepwise heating analyses: samples were irradiated in the TRIGA reactor at Pavia
90 University (Italy) without Cd shielding so as not to lose information on Cl. Fast neutron flux was
91 monitored by use of MMhb standard hornblende ($523.1 \pm 4.6 \text{ Ma}$; Renne *et al.*, 1998). Stepwise
92 heating data, including the J factor, are given in Table 2. Interference and production factors for Ca,
93 Cl and K were: $(^{39}\text{Ar}/^{37}\text{Ar})_{\text{Ca}} = 0.00068$; $(^{38}\text{Ar}/^{37}\text{Ar})_{\text{Ca}} = 0.00025$; $(^{36}\text{Ar}/^{37}\text{Ar})_{\text{Ca}} = 0.00027$;
94 $(^{40}\text{Ar}/^{39}\text{Ar})_{\text{K}} = 0.007$. Ar isotope analyses were done at the Institut für Geologie, Universität Bern,
95 using an all-metal extraction line attached to a double-vacuum resistance oven and a thermocouple
96 on the external part of the crucible. Furnace blanks yielded an atmospheric composition; ^{40}Ar
97 blanks had atmospheric composition and ranged from 4.5 pL/min at 700°C to 14.3 at 1000°C . K, Ca
98 and Cl concentrations and ratios were determined from the ^{39}Ar , ^{37}Ar and ^{38}Ar release.

99

100

The serendipitous start

101

102 The original impetus for the present investigation was not an examination of the suitability of the
103 B4M “standard”. This material is no longer widely used in the geochronological community. On the

104 contrary, its presumed chemical uniformity and its availability (tens of g) made it an attractive
105 starting material for a simple test for a completely different purpose.

106 Rb-Sr analyses of clastic sediments sometimes require that the fine-grained “clay fraction” be
107 separated from them. Because the separation normally occurs by grinding the rock, followed by
108 Stokes’ Law settling in Atterberg cylinders containing distilled water, it is desirable to ascertain
109 whether Rb is mobilised in the course of this procedure. The smallest grain sizes require the longest
110 settling times, therefore it is conceivable that if such a Rb leaching occurs, there could be a cutoff
111 grain size above which the shorter settling time and the smaller surface/volume ratio ensure that the
112 effect is negligible.

113 Our initial test was performed by treating the (presumably homogeneous) muscovite as if it were a
114 clastic sediment, subjecting it to comminution and separation of the fine fraction by settling in
115 water. The expected behaviour of the size fractions is sketched in Fig. 1a. The Sr isotopic
116 composition is expected to be always constant. The Rb/Sr ratio, reflecting the greater solubility of
117 Rb hosted in the mica interlayer positions, may decrease as the analysed grain size decreases.
118 Whether leaching occurs, and at what point it becomes statistically significant, can be directly
119 evaluated by a plot such as Fig. 1a. Results are given in Table 1 and Figure 1b.

120 The sample did not behave as expected.

121

122

123

X-ray diffractometry

124

125 The reason for the Sr isotopic heterogeneity (Fig. 1b) could conceivably be due to diffusive
126 exchange of Sr between a mineralogically homogeneous mica and the whole rock matrix, or to Sr
127 inheritance in a mineralogically heterogeneous mica. However, the former would result in a single
128 point, as all grain sizes A-E are just a laboratory comminution of exactly the same 300-500 μm
129 grains. No significant variation amongst the ground fractions A-E should thus be observed,

130 irrespective of any possible zonation in the starting material (the large grains before grinding). The
131 pattern of the data in Fig. 1b is not explained by Sr exchange as the dominant effect.
132 This leaves mineralogical heterogeneity as the most plausible explanation; we assessed it with X-
133 ray diffraction (XRD). The resulting spectra showed a monotonic increase of the phengite peaks in
134 the smaller fractions. Only spectra A and E, showing the highest contrast, are shown for clarity
135 (Fig. 2). The unambiguous observation is that grinding under ethanol achieved a physical separation
136 between white mica varieties with different mechanical resistance. While the phengite is purified by
137 grinding and concentrated in the finest size fraction A, its mass fraction is not modified by our
138 treatment. Once we know what to look for, phengite is also very prominent in the electron
139 microprobe analyses of the untreated grains (see following paragraph and Fig. 3a). The total mass
140 fraction of phengite in the untreated 300-500 μm grains is probably near 30-40 %.

141

142

143

Electron microprobe analyses

144

145 162 spot analyses were acquired on randomly selected locations in random grains, including several
146 series of 2-10 analyses in the same grain. Results are shown in Table 2 and Fig. 3, calculated as
147 atoms per formula unit (apfu) using a 24 oxygen atoms normalisation.

148 By far the most important result is that all analyses have stoichiometric K concentrations. This is
149 conclusive proof that the separate does not contain altered grains.

150 The XRD observation discussed in the previous paragraph and presented in Fig. 2 is confirmed by
151 the microprobe data. Si concentrations range between 6.6 and 7.2 apfu, *i.e.* between a muscovitic
152 and a phengitic composition (Fig. 3a). However, other major elements reveal additional
153 information, which would be overlooked in a simple diagram such as Fig. 3a. Diagrams in Figs. 3b-
154 c are plotted as common-denominator ratios (*cf.* Villa 2001, his Fig. 2) because the choice of a
155 common denominator allows binary mixtures to be revealed as lines, ternary ones as triangles, and

156 n-ple mixtures as n-polygons (which can be non-planar for $n \geq 4$; in this case, the number of
157 vertices is easier to recognize if the data are plotted in three dimensions, or in orthogonal 2-
158 dimensional projections).

159 Figs. 3b and 3c show the intra-grain distributions of Mg, Fe, Na and F. The point analyses define a
160 very wide and varied distribution of these elements within the grains. The minimum polygon
161 enclosing the data points is a quadrangle, whose vertices can be traced to distinct white mica
162 generations. Vertices P, Q, R and S are defined by the same analysis spots in both figures. P is a
163 muscovite with Si = 6.6 atoms per formula unit (apfu), with no F, high Na, and low Mg/Fe; its
164 closest representatives are spots flat59 and flat55 (Table 2). Q is a muscovite with Si = 6.73 apfu,
165 high F, intermediate Na, and intermediate Mg/Fe. Its closest representatives are spots flat51 and
166 flat52. R is a phengite with no F, low Na, and intermediate Mg/Fe; it is represented by spot vert92.
167 S is a phengite with high F/Fe, intermediate Na, and high Mg/Fe. Its closest representatives are
168 spots flat19 and vert39.

169 The ca. 150 points in the interior of the quadrangle do not represent each a different mica
170 generation. Because they lie in the interior, they can be viewed as mixtures of the vertex micas.
171 They merely attest to the fact that the ca. 5 μm spatial resolution of the electron microprobe is
172 insufficient to resolve the scale at which the four micas replace each other in the B4M sample (*cf.*
173 an example of presumably similar, but coarser, mica intergrowths in Villa 2006, his Fig. 3). If the
174 beam size of the electron microprobe had been smaller than the size of the individual phengite and
175 muscovite domains, we would have obtained only four discrete, tight clusters coincident with the
176 four vertices. The observation that most points lie well inside the quadrangle shows instead that the
177 vast majority of analyses straddled at least two boundaries separating at least three different mica
178 generations, each smaller than the beam diameter of 5 μm .

179 We attempted to correlate the B4M separate with a rock, so as to be able to identify microtextures
180 and reaction sequences leading to the presently observed polymetamorphic relicts. A thin section
181 was prepared from gneiss hand specimen G-1 from the teaching collection, whose quarry of

182 provenance is the same as the 1961 collection by Jäger *et al.* (1963). Back-scattered electron maps
183 of G-1 reveal sector replacement textures rather than simple core-rim overgrowths. However, the
184 inventory of the white mica generations differs from that of the B4M separate. G-1 only shows Si <
185 6.96 (Table 2) and contains one point with a very high Na/Mg, but lacks the high F/Mg and the low
186 Na/Mg micas (Fig. 3d) that account for 25 % of the values that we observed in the separate (Fig.
187 3c). We conclude that G-1 is similar, but not identical, to the still elusive source rock of the B4M
188 separate. A more detailed search among all possible lithologies extracted over 50 years from the
189 Brione quarry exceeds the scope of this work and would not modify our petrological and
190 geochronological conclusions. Pressure and temperature could be constrained more tightly if we
191 had had the rock, but even with just the separate it is quite obvious that phengite and muscovite are
192 in disequilibrium.

193 A comparison of the orientation (vertical vs flat) in the grain mount is shown in Fig. 3c. The two
194 distributions are broadly similar; this means that the direction of the mount does not lead to
195 artefacts overwhelming the main petrological conclusion. Both populations cover overlapping areas
196 of the diagram, which (as we already mentioned) is evidence that the phengite-muscovite retrograde
197 intergrowths are more narrowly spaced than the size of the electron beam excitation volume
198 (approximately 2 μm deep and 5 μm in diameter). In detail, however, we also note that the flatly
199 bedded grains are slightly shifted towards the “muscovite line”, PQ, while the vertical grains cluster
200 preferentially closer to the “phengite line”, RS. This may mean that in the vertically mounted
201 grains, whose interior is immediately exposed to the electron beam, the mass proportion of the
202 intergrown layers is more favourable to the two phengites R and S, while in the flat-lying mount,
203 which preferentially exposes the external part of each grain to the electron beam, it is the latest
204 accretion/substitution/retrogression that predominates.

205 The major element data thus require that at least four generations of white mica were present in the
206 rock from which the distributed separate was prepared. The petrogenetic significance of each of

207 these generations remains elusive until a duplicate of the lithology sampled by Jäger *et al.* (1963)
208 will be subjected to a modern textural, microchemical and petrological study.

209

210

211 **Rb-Sr and ³⁹Ar-⁴⁰Ar geochronology**

212

213 The five Rb-Sr analyses (Fig. 1b) do not define a single isochron line. Similarly, the ⁸⁷Sr/⁸⁶Sr vs
214 1/Sr diagram (Fig. 4) is incompatible with a binary mixing between a “common” and a “radiogenic”
215 Sr reservoir. Instead, the minimum polygon enclosing all points and having vertices with $x > 0$ is a
216 quadrangle. This confirms that the four mica generations identified by electron microprobe have
217 distinct Sr isotope systematics. The two coarse fractions D and E (*i.e.* the muscovitic mica
218 identified by XRD in Fig. 2) are likely to be petrologically closer to each other than the finer size
219 fractions. Since there is no way to reconstruct the paragenesis in petrological equilibrium with the
220 muscovite(s) or to recover the minerals forming it, we regressed fractions D and E together. Their
221 apparent Rb-Sr age is 14.8 ± 0.2 Ma (using the decay constant $\lambda_{87} = 1.397 \times 10^{-11} \text{ a}^{-1}$, Rotenberg *et al.*
222 *al.* 2012, indistinguishable from that proposed by Nebel *et al.* 2011, $\lambda_{87} = 1.393 \times 10^{-11} \text{ a}^{-1}$). The
223 three fine-grained fractions A, B and C, which contain increasing mass fractions of phengitic mica
224 (Fig. 2), obviously give a meaningless isochron if regressed with the retrograde muscovite;
225 moreover, the three-point isochron (with an unweighted apparent Rb-Sr age of 19.2 ± 4.5 Ma) has a
226 high MSWD of 17. These ages are not well founded and must not be used to infer the petrogenetic
227 history of the B4M gneiss. However, it is worth noticing that the different trends in Figs. 1b and 4
228 are evidence of four unrelated components that are preserved in the Sr isotopic record.

229 Two fractions, A and E, were irradiated and analysed by ³⁹Ar-⁴⁰Ar stepwise heating. The data are
230 presented in Table 3 and visualised in Fig. 5. The age spectra (Fig. 5a) suggest apparent ages
231 around 17-18 Ma, with fine-grained phengite (identified by the step with the lowest Cl/K ratio, see
232 below) significantly older than coarse-grained muscovite. However, as pointed out by Allaz *et al.*

233 (2011), age spectra only display a small fraction of the information provided by Ar isotope
234 systematics. The Ca/K ratio (Fig. 5b) identifies the phengite (fraction A) as virtually Ca-free, while
235 fraction E evidently contains a detectable paragonitic component. The age-Cl/K common
236 denominator three-isotope correlation diagram (Fig. 5c) provides further clarity by identifying a Cl-
237 rich phase (a retrogressive mica younger than 10 Ma) and two different Cl-poor micas.

238 One cause of concern is the relative importance of recoil artefacts (Villa 1997) due to the sub- μm
239 grain size of sample A. Its age is expected to be elevated by ^{39}Ar recoil loss during irradiation. In
240 order to evaluate whether ^{39}Ar recoil was the predominant cause for the elevated age of sample A,
241 we can exploit the fact that the recoil of radiogenic ^{40}Ar and of artificial Cl-derived ^{38}Ar is much
242 smaller than that of ^{39}Ar (Onstott *et al.* 1995). Therefore, the effects of recoil would manifest
243 themselves by shifting steps along the dashed green line with positive slope in Fig. 5c. The
244 observed pattern does not conform to this expectation. This means that ^{37}Ar and ^{39}Ar recoil,
245 although they were present, did not overwhelm the true diachronism and true Ca/Cl variations due
246 to the mineralogical, chemical and isotopic heterogeneities described above.

247 We also note that the present observations were possible because the Rb-Sr apparent age difference
248 of 4 Ma between phengite and muscovite amounts to a $> 20\%$ effect. If, instead of the Oligocene
249 B4M sample, we had performed our serendipitous clay settling test with the Archean
250 Rhenosterkopjes muscovite (Nägler and Villa 2000), the resulting age heterogeneity would have
251 been barely resolvable without the *a priori* knowledge of what to look for.

252

253

254

Other natural reference materials

255

256 To date, our work on the B4M separate is the first dedicated microchemical documentation of the
257 extent to which natural materials used by the geochronological community as calibrators actually
258 fulfill the requirements of homogeneity (VIM, 2008, entry 5.13). There have been reports of

259 significant chemical heterogeneities in the Fish Canyon sanidine (Bachmann et al. 2002, their Figs.
260 10 through 15), the MMhb1 hornblende (Villa et al. 1996) and, indirectly, in the GA 1550 biotite
261 (Hall 2013). The Fish Canyon sanidine has also been studied by Dazé et al. (2003, their Appendix
262 A), who document a broad (albeit imprecise) correlation of single grain stepheating ages with
263 chemical composition. This means that, even at the single handpicked grain level, there are several
264 percent of the Ar that are hosted by a heterochemical contaminant having a resolvably different age.
265 This is only to be expected if one takes into account the petrological groundwork by Bachmann et
266 al. 2002.

267 The GA 1550 biotite was not studied as extensively as would be desirable by electron microprobe.
268 The large variations of the Ca/K ratios during stepheating and the anomalies of the recoil patterns of
269 ^{37}Ar , ^{38}Ar and ^{39}Ar (Hall 2013) are evidence that about 10 % of the ^{39}Ar release is associated with
270 Ca-rich impurity phases and probably also with secondary phyllosilicates.

271 It is clear that there is very ample room for augmenting the desperately needed documentation of
272 natural materials by extensive microchemical groundwork. It is hoped that if the quest will cover a
273 sufficient number of natural samples there may be one that will be found to be homogeneous at the
274 percent level. This will be the prerequisite for decreasing the minimum sample size required to
275 ensure the homogeneity necessary for calibration work.

276

277

278

Jaegerism reassessed

279

280 The original assumption regarding the distributed B4M separate, that it consists of 300-500 μm
281 sized homogeneous grains, is not verified by our electron microprobe data. In actual fact, the
282 “large” grains consist of phengite-muscovite intergrowths smaller than 5 μm . These heterochemical
283 retrogression products comprise several (at least four, but the true number is actually irrelevant,
284 provided it is higher than one) mica generations, whereof at least three are relicts. The crucial

285 geochronological implication is that these diachronic mica generations never underwent complete
286 diffusive reequilibration, even at $T > 600$ °C, and thus preserve an isotopic disequilibrium. Because
287 a phengite does NOT transform to muscovite by temperature and pressure alone, as they are not
288 isochemical, it means that petrological disequilibrium in B4M is the record of several fluid
289 circulation events in a chemically open system. We observe that metamorphic peak temperatures of
290 ca. 635 °C (which occurred during the Miocene regional thermal peak in the Central Alps: Janots et
291 al. 2009, Allaz et al. 2011) were insufficient to erase the petrological heterogeneities by completely
292 recrystallising the two relict high-pressure phengite generations (probably of Eocene age: Gebauer
293 1999, p. 193). As a consequence of petrologic disequilibrium, the Sr and Ar isotopic systems
294 preserve an isotopic inheritance (*cf.* Villa 1998). This supports the conclusions by Allaz *et al.*
295 (2011) that the “closure temperature” at which the K-Ar system in white mica is reset during
296 regional metamorphism (and ensuing medium-slow exhumation and cooling) exceeds 500 °C.
297 Furthermore, the isotopic disequilibrium is equally well developed in Sr and Ar. This negates the
298 working hypothesis by Purdy and Jäger (1976) that Ar is orders of magnitude more mobile than Sr
299 in the mica structure.

300

301

302

Conclusions

303

304 Petrology controls the Sr and Ar isotopic record of the B4M separate. A number of retrograde
305 reactions have superimposed several mica generations, which were intergrown with the preceding
306 one(s) without completely replacing them. The fact that high-temperature regional metamorphism
307 did not achieve Ar and Sr isotopic homogenisation, is a further confirmation that relicts are a
308 guarantee of isotopic inheritance. This unambiguously requires that only total recrystallisation, and
309 not just heating to 635 °C, is the necessary condition to completely reset the Sr and Ar clocks.

310 The implications for the choice of a natural reference material are manifold.

311 The chemical homogeneity (VIM 2008, entry 5.13) at the μm scale is a *sine qua non* condition for
312 the selection of a natural reference material, as microchemical inhomogeneity is normally
313 associated to isotopic disequilibrium. Chemical homogeneity is easily assessed by electron
314 microprobe. Even if the true scale of the chemical heterogeneity is smaller than the spatial
315 resolution of the electron beam, the present work has shown that averaging small heterogeneous
316 mica volumes results in a detectable heterogeneity of the electron microprobe analyses.

317 A stronger requirement, that of petrologic equilibrium, would ensure that the isotopic age be free of
318 retrogression and recrystallisation disturbances. This is probably a necessary requirement for an
319 acceptable natural reference material, as it is not easy to imagine a mineral geochronometer that
320 achieved and preserved complete chemical and isotopic homogeneity all while its host rock did not.
321 The choice criterion of “slow/fast cooling” is irrelevant, as temperature had a subordinate influence
322 in setting the isotope record of B4M. Instead, a natural reference material must be free of
323 retrogression reactions at the sub- μm scale.

324

325

326

Acknowledgements

327

328 This work was funded by Institut für Geologie, Universität Bern. The electron microprobe was
329 funded by Schweizerischer Nationalfonds grant 200021-103479/1. Constructive reviews by two
330 unnamed referees, and editorial handling by F. Jourdan, are gratefully acknowledged.

331

332

333

References

334

335 ALLAZ, J., BERGER, A., ENGI, M. & VILLA, I.M. 2011. The effects of retrograde reactions and of
336 diffusion on ^{39}Ar - ^{40}Ar ages of micas. *Journal of Petrology*, **52**, 691-716.

337 BACHMANN, O., DUNGAN, M.A. & LIPMAN, P.W. 2002. The Fish Canyon magma body, San Juan
338 volcanic field, Colorado: rejuvenation and eruption of an upper-crustal batholith. *Journal of*
339 *Petrology*, **43**, 1469-1503.

340 DAZÉ, A., LEE, J.K.W. & VILLENEUVE, M. 2003. An intercalibration study of the Fish Canyon
341 sanidine and biotite $^{40}\text{Ar}/^{39}\text{Ar}$ standards and some comments on the age of the Fish Canyon
342 Tuff. *Chemical Geology*, **199**, 111-127.

343 DODSON, M.H. 1986. Closure profiles in cooling systems. *Materials Science Forum*, **7**, 145-154.

344 FLISCH, M. 1982. Potassium-argon analysis. In: Odin, G.S. (ed.), Numerical dating in stratigraphy.
345 Wiley, Chichester, 151-156.

346 GEBAUER, D. 1999. Alpine geochronology of the Central and Western Alps: new constraints for a
347 complex geodynamic evolution. *Schweizerische Mineralogische und Petrographische*
348 *Mitteilungen*, **79**, 191-208.

349 HALL, C.M. 2013. Direct Measurement of Recoil Effects on Ar-Ar Standards. In: Jourdan, F.,
350 Mark, D. & Verati, C. (eds) $^{40}\text{Ar}/^{39}\text{Ar}$ dating: from geochronology to thermochronology, from
351 archaeology to planetary sciences. *Geological Society of London Special Publications*, this
352 volume

353 JÄGER, E. 1962. Rb-Sr age determinations on micas and total rocks from the Alps. *Journal of*
354 *Geophysical Research*, **67**, 5293-5306.

355 JÄGER, E. 1967. Kritische Betrachtungen zur Interpretation der Alterswerte. In: Jäger, E., Niggli, E.
356 & Wenk, E., Rb-Sr Altersbestimmungen an Glimmern der Zentralalpen. *Beiträge zur*
357 *Geologischen Karte der Schweiz*, **NF 134**, 38-40.

358 JÄGER, E. & FAUL, H. 1959. Age measurements on some granites and gneisses from the Alps.
359 *Bulletin of the Geological Society of America*, **70**, 1553-1557.

360 JÄGER, E., NIGGLI, E. & BAETHGE, H. 1963. Two standard minerals, biotite and muscovite, for Rb-
361 Sr and K-Ar age determinations, sample Bern 4B and Bern 4M from a gneiss from Brione,

362 Valle Verzasca (Switzerland). *Schweizerische Mineralogische und Petrographische*
363 *Mitteilungen*, **43**, 465-470.

364 JANOTS, E., ENGI, M., RUBATTO, D., BERGER, A., GREGORY, C. & RAHN, M.K. 2009. In-situ
365 determination of heating rates in collisional orogeny. *Geology*, **37**, 11-14.

366 NÄGLER, T.F & VILLA, I.M. 2000. In pursuit of the ^{40}K branching ratio: K-Ca and ^{39}Ar - ^{40}Ar dating
367 of gem silicates. *Chemical Geology*, **169**, 5-16.

368 NEBEL, O., SCHERER, E.E. & MEZGER, K. 2011. Evaluation of the ^{87}Rb decay constant by age
369 comparison against the U-Pb system. *Earth and Planetary Science Letters*, **301**, 1-8.

370 ONSTOTT, T.C., MILLER, M.L., EWING, R.C., ARNOLD, G.W. & WALSH, D.S. 1995. Recoil
371 refinements - implications for the $^{40}\text{Ar}/^{39}\text{Ar}$ dating technique. *Geochimica et Cosmochimica*
372 *Acta*, **59**, 1821-1834.

373 PURDY, J. & JÄGER, E. 1976. K-Ar ages on rock-forming minerals from the central Alps. *Memorie*
374 *dell'Istituto di Geologia e Mineralogia dell'Università di Padova*, **30**, 31 pp

375 ROTENBERG, E., DAVIS, D.W., AMELIN, Y., GHOSH, S. & BERGQUIST, B.A. 2012. Determination of
376 the decay-constant of ^{87}Rb by laboratory accumulation of ^{87}Sr . *Geochimica et*
377 *Cosmochimica Acta*, **85**, 41-57.

378 TODD, C.S. & ENGI, M. 1997. Metamorphic field gradients in the Central Alps. *Journal of*
379 *Metamorphic Geology*, **15**, 513-530.

380 VILLA, I.M. 1997. Direct determination of ^{39}Ar recoil range. *Geochimica et Cosmochimica Acta*,
381 **61**, 689-691

382 VILLA, I.M. 1998. Isotopic Closure. *Terra Nova*, **10**, 42-47.

383 VILLA, I.M. 2001. Radiogenic isotopes in fluid inclusions. *Lithos*, **55**, 115-124.

384 VILLA, I.M. 2006. From the nm to the Mm: isotopes, atomic-scale processes, and continent-scale
385 tectonic models. *Lithos*, **87**, 155-173.

- 386 VILLA, I.M. 2010. Disequilibrium Textures vs Equilibrium Modelling: Geochronology at the
387 Crossroads. In: Spalla, M.I., Marotta, A.M. & Gosso, G. (eds) Advances in interpretation of
388 geological processes. *Geological Society of London Special Publications*, **332**, 1-15.
- 389 VILLA, I.M., GROBÉTY, B., KELLEY, S.P., TRIGILA, R. & WIELER, R. 1996. Assessing Ar transport
390 paths and mechanisms for McClure Mountains Hornblende. *Contributions to Mineralogy and*
391 *Petrology*, **126**, 67-80.
- 392 VILLA, I.M., RUGGIERI, G., PUXEDDU, M. & BERTINI, G. 2006. Geochronology and isotope transport
393 systematics in a subsurface granite from the Larderello-Travale geothermal system (Italy).
394 *Journal of Volcanology and Geothermal Research*, **152**, 20-50.
- 395 VIM 2008. The International Vocabulary of metrology – Basic and general concepts and associated
396 terms, 3rd edition, JCGM 200:2008, <http://www.bipm.org/en/publications/guides/vim.html>

Figure Captions

- 397
- 398
- 399
- 400
- 401 Fig. 1 – (a) Expected behaviour of homogeneous minerals ground and separated by settling in
402 distilled water. The coarsest grain sizes settle first and their Rb/Sr ratio is not modified. Smaller
403 grains might (but need not), due to a combination of higher surface/volume ratios and longer
404 settling times, experience Rb leaching and follow a trajectory towards the left. The trajectory is
405 horizontal, as the $^{87}\text{Sr}/^{86}\text{Sr}$ ratio is constant. – (b) Observed behaviour of ground B4M separate.
- 406 Fig. 2 – X-ray diffraction spectra of coarsest fraction B4M-E and finest fraction B4M-A. The
407 characteristic lines of phengite are shown in orange above the diagram. Phengite is present in
408 B4M-A but absent in B4M-E, which only consists of muscovite.
- 409 Fig. 3 – Electron microprobe results (apfu) on grain mounts of the untreated B4M separate as
410 distributed. All analyses have white mica compositions. Filled circles, ‘flat’ grain mount; open
411 triangles, ‘vertical’ grain mount. (a) Si vs (Al+Fe+Mg), showing increasing Si substitution

412 from muscovitic towards more phengitic compositions of white mica(s). (b) F-Mg-Fe three-
413 element common-denominator correlation diagram. At least four end-members are required:
414 two muscovites, P and Q, and two phengites, R and S. (c) Na-F-Mg three-element common-
415 denominator correlation diagram. End-members are defined by the same spots (see Table 2) as
416 in Fig. 3b. (d) Electron microprobe results on thin section of whole rock from Brione quarry.
417 The field overlaps with that of the grain mounts in Fig. 3c, but spans less compositional
418 variety. The whole rock and the grain mount are not the same sample.

419 Fig. 4 - $^{87}\text{Sr}/^{86}\text{Sr}$ vs $1/\text{Sr}$ (ppm^{-1}) diagram. The minimum polygon enclosing all points and having
420 vertices with $x > 0$ is a quadrangle. This requires at least four distinct Sr reservoirs.

421 Fig. 5 - ^{39}Ar - ^{40}Ar stepwise heating results for size fractions A and E. (a) Age spectra. The older age
422 of A could be, at least to some extent, a recoil artefact. (b) Ca/K spectra. A paragonitic white
423 mica is visible in coarse fraction E, but not in fine fraction A. (c) Three-isotope common-
424 denominator correlation diagram. The trajectory of size fraction A (red triangles) contradicts
425 recoil as the predominant factor (green dashed line). Size fraction E (blue circles) has higher
426 Ca/K ratios (Table 3), evidence of a paragonitic component absent in size fraction A.

427

428

429

Table Captions

430

431 Table 1 – Rb-Sr results on size fractions of ground “muscovite standard” B4M. Nominal grain
432 sizes: A, $< 0.6 \mu\text{m}$; B, $0.6\text{-}2 \mu\text{m}$; C, $2\text{-}6 \mu\text{m}$; D, $6\text{-}20 \mu\text{m}$; E, $> 20 \mu\text{m}$.

433

434 Table 2 – Electron microprobe results on two grain mounts of the unprocessed B4M separate as
435 distributed and on a whole-rock thin section of Brione gneiss from the teaching collection of the
436 Universität Bern. ‘flat’, grains that were mounted parallel to the $\{001\}$ plane; ‘vert’, grains that

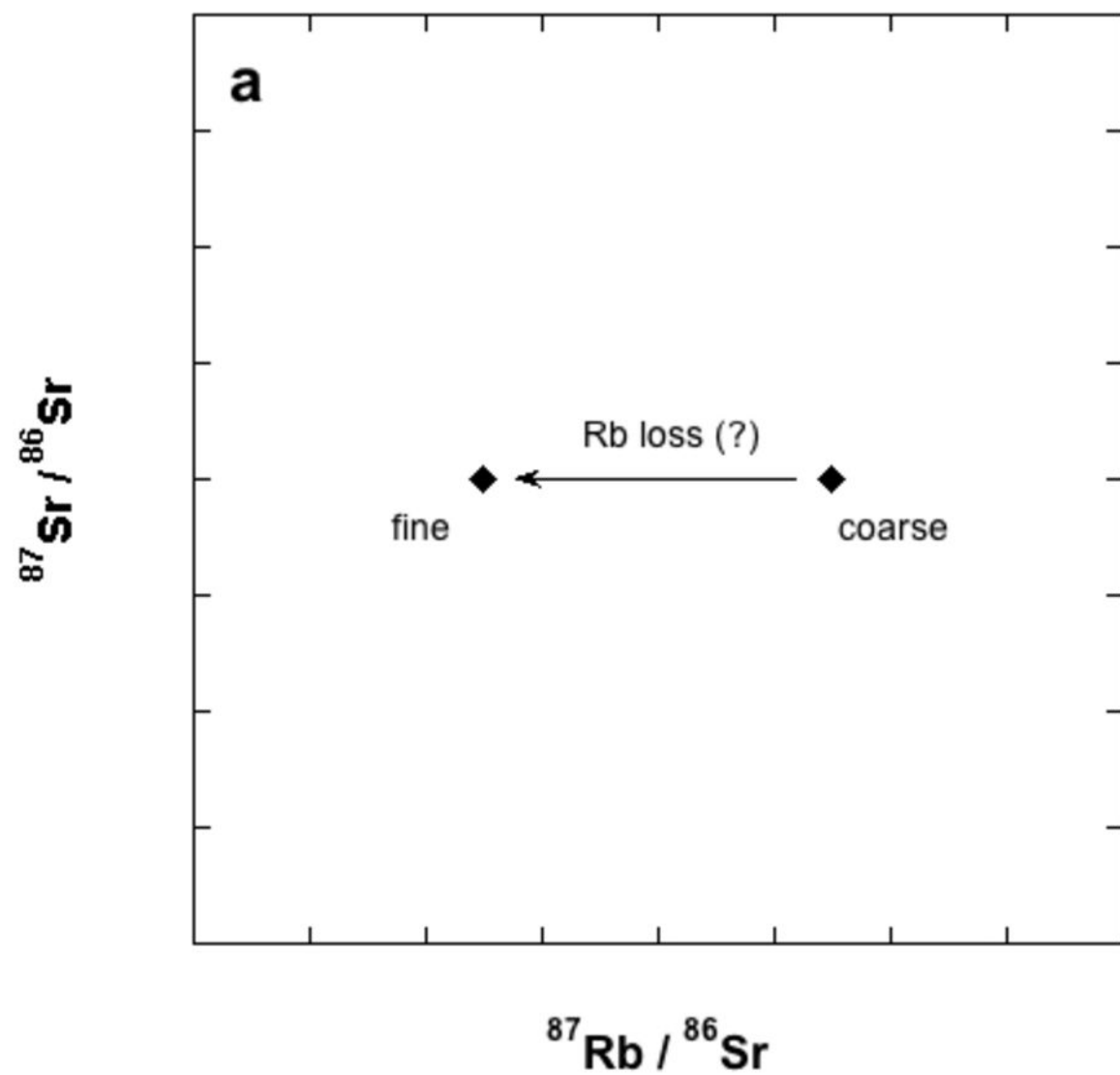
437 were mounted perpendicularly to it; 'WR', point analyses from the thin section. Analyses that did
438 not sum up to 100 %, or that were clearly not muscovite, were omitted.

439

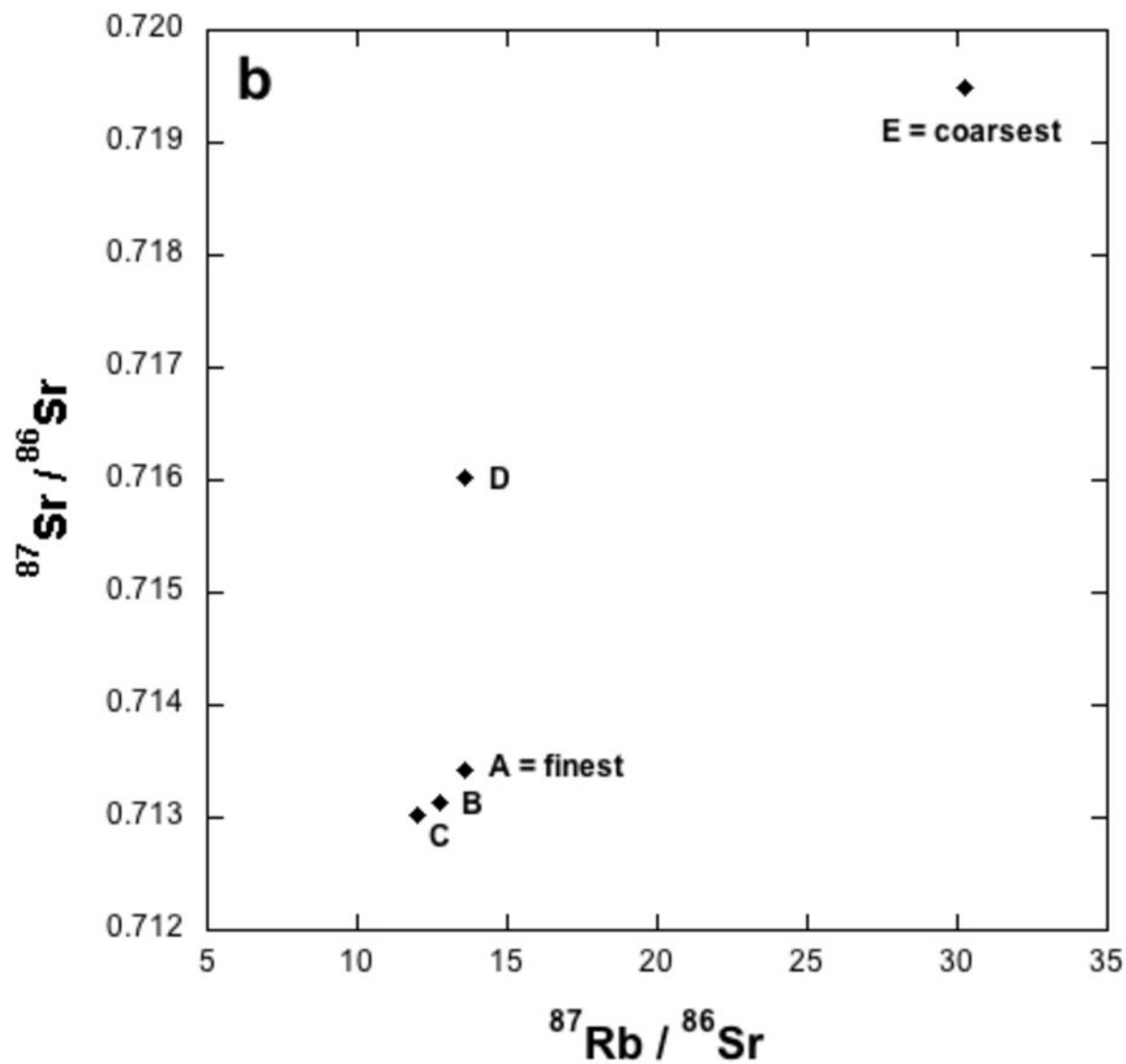
440 Table 3 – ^{39}Ar - ^{40}Ar stepheating analyses on size fractions A and E (labels as in Table 1). All

441 isotopes are in mL. Uncertainties are 1 standard deviation.

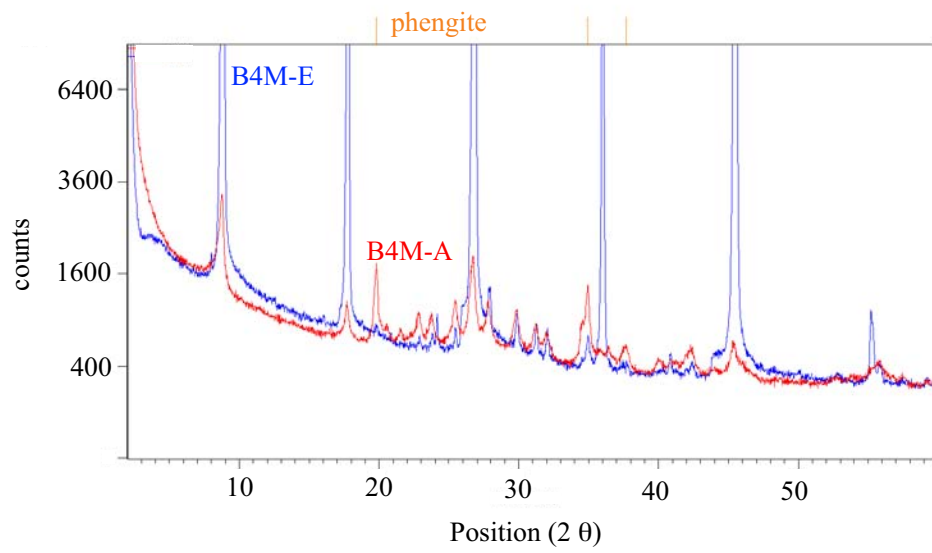
Heri et al. Fig.1a



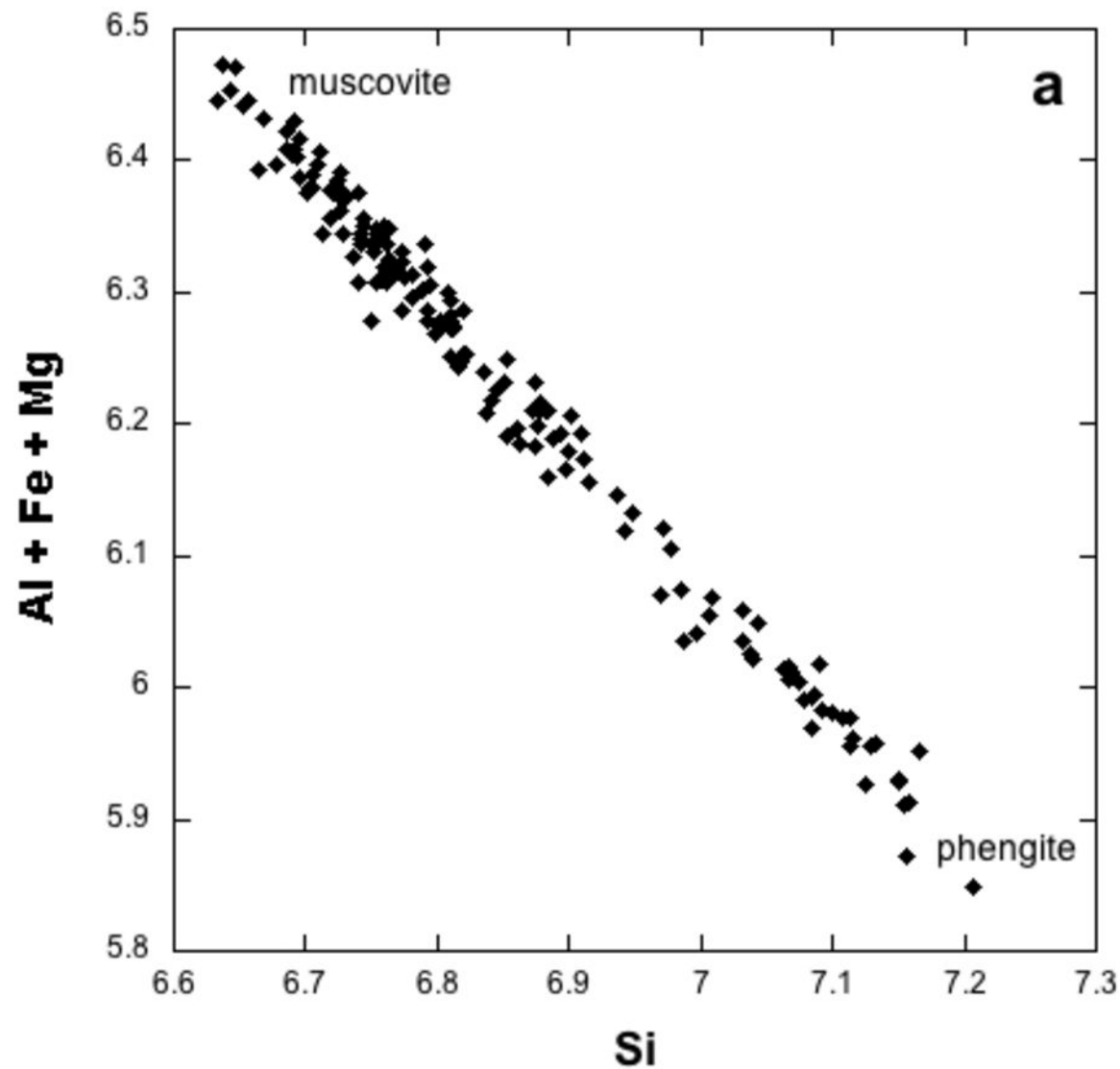
Heri et al. Fig.1b



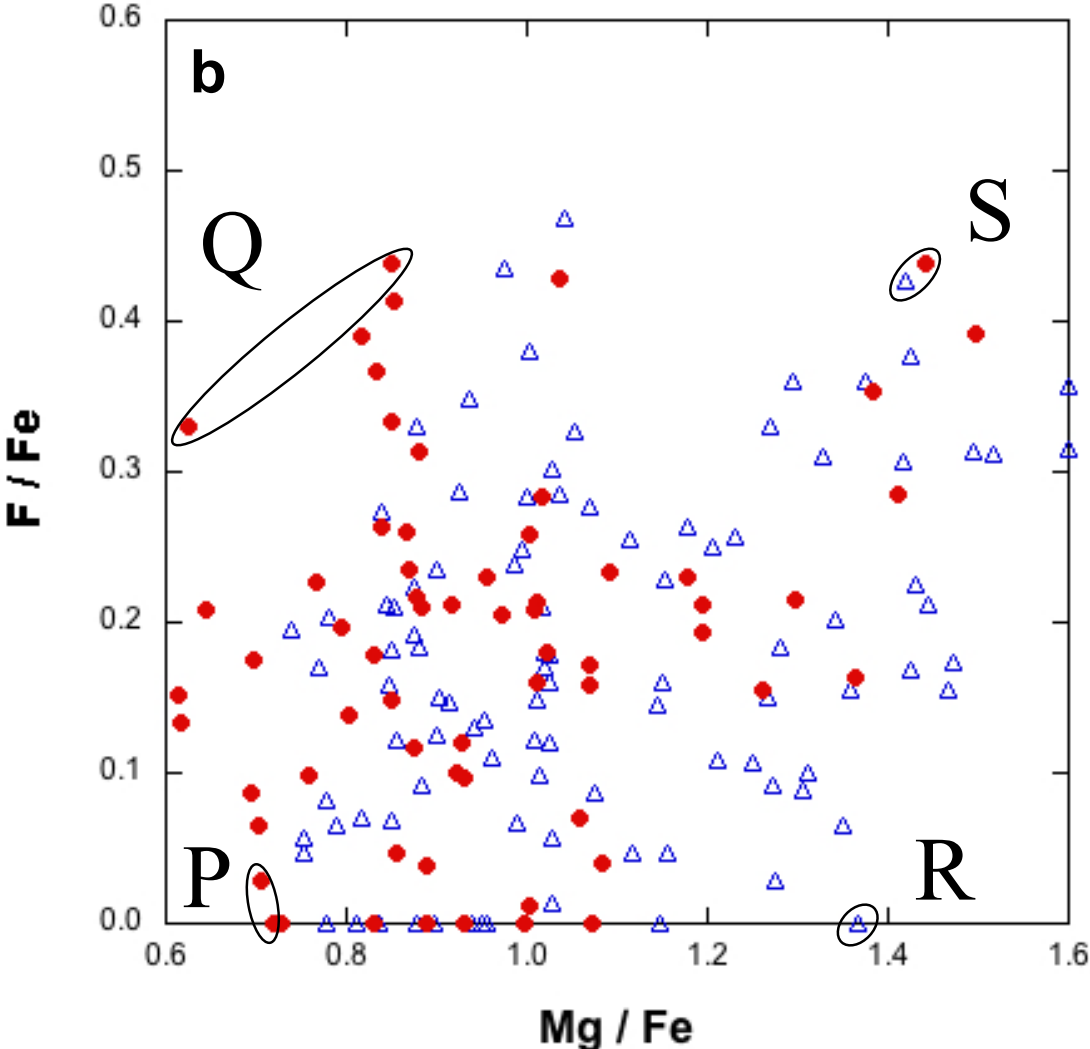
Heri et al. Fig.2



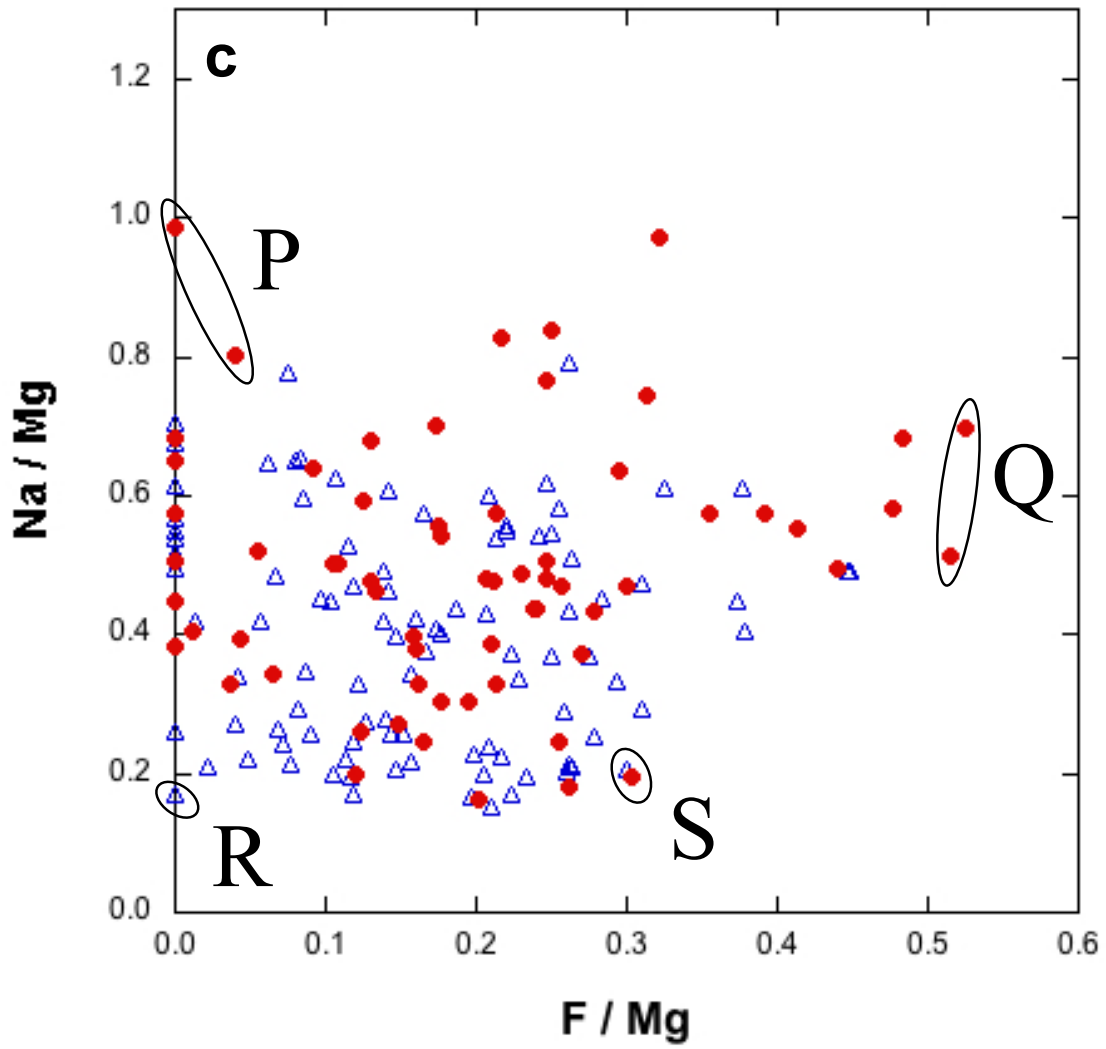
Heri et al. Fig.3a



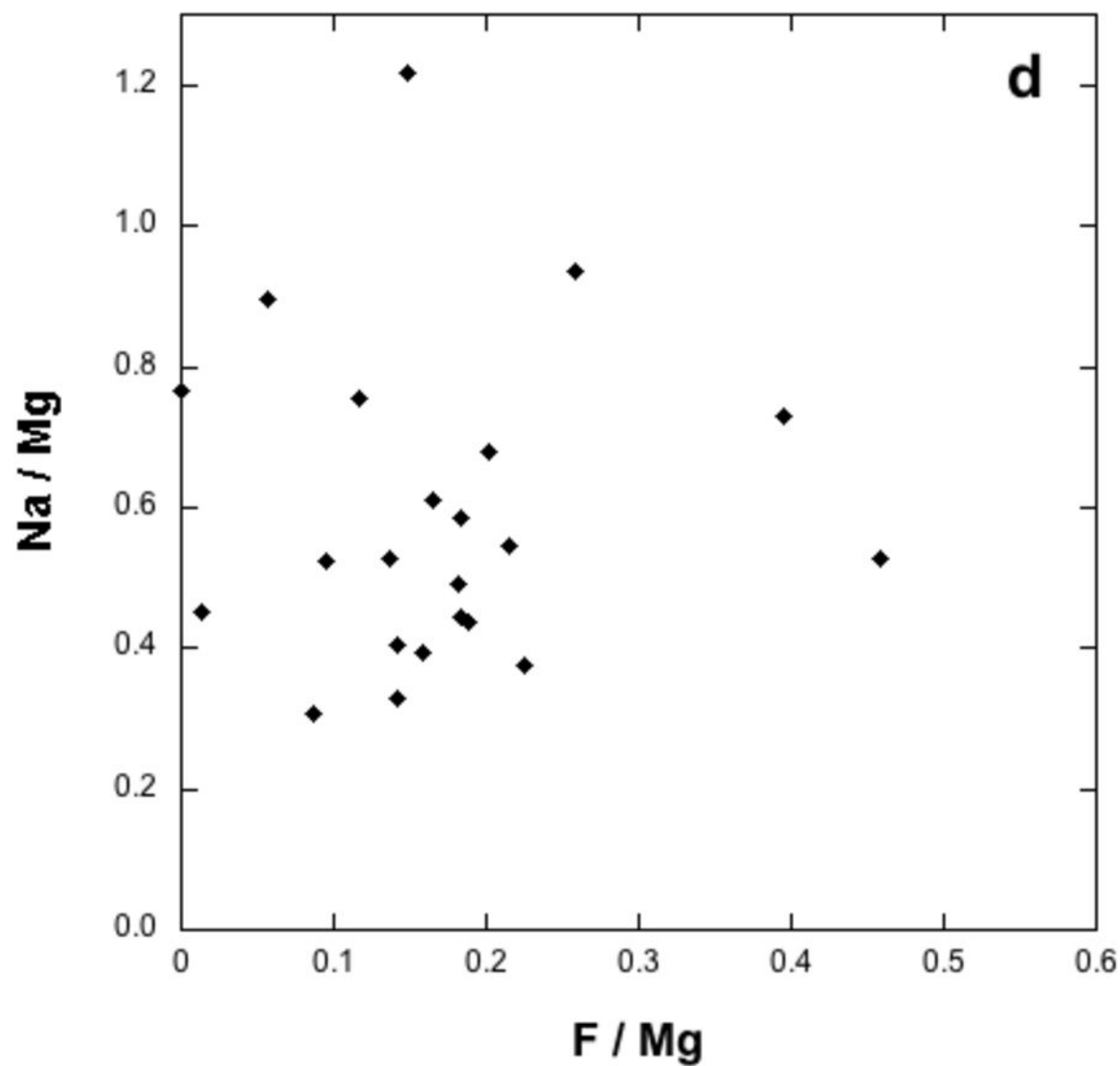
Heri et al. Fig.3b



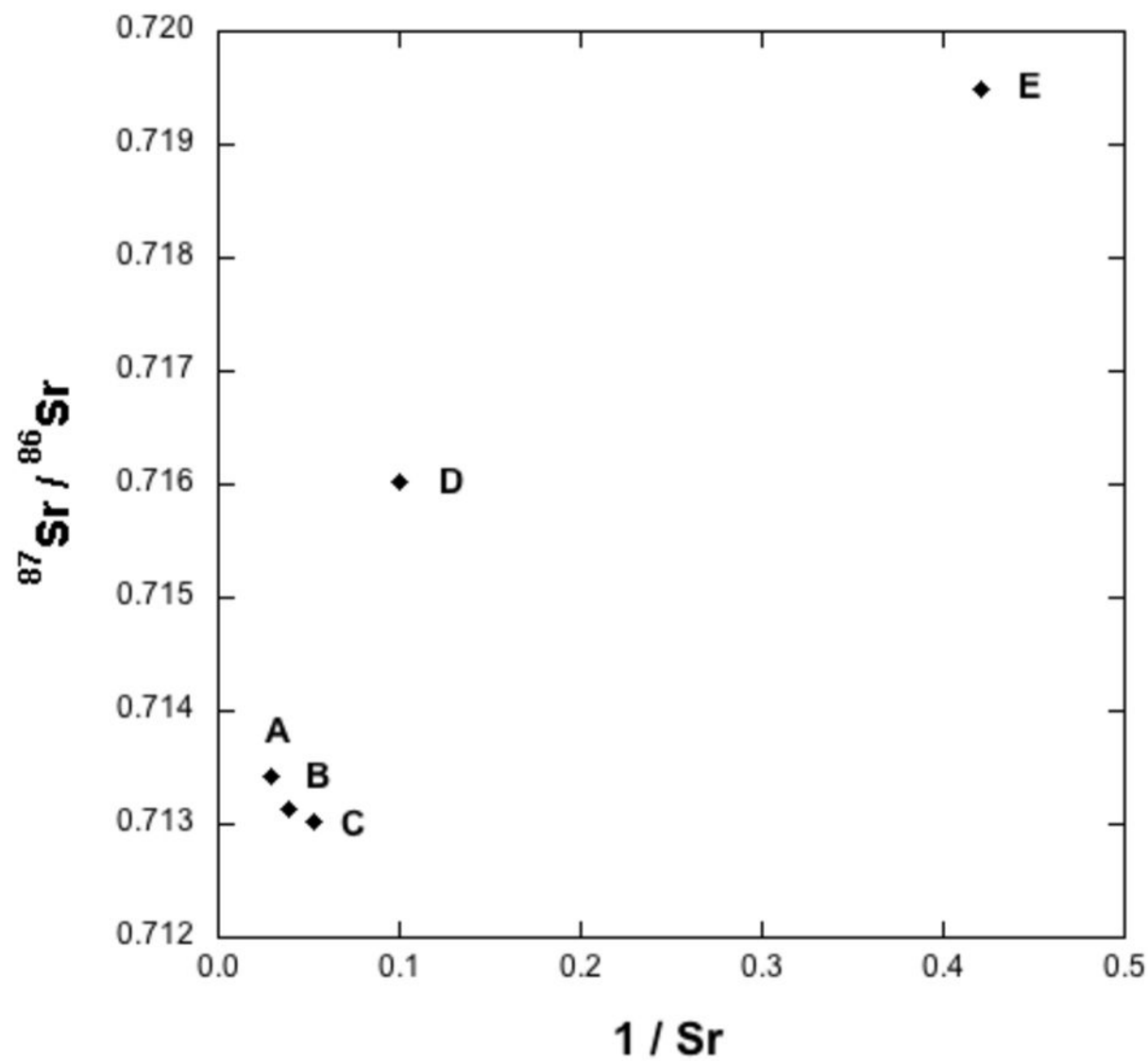
Heri et al. Fig.3c



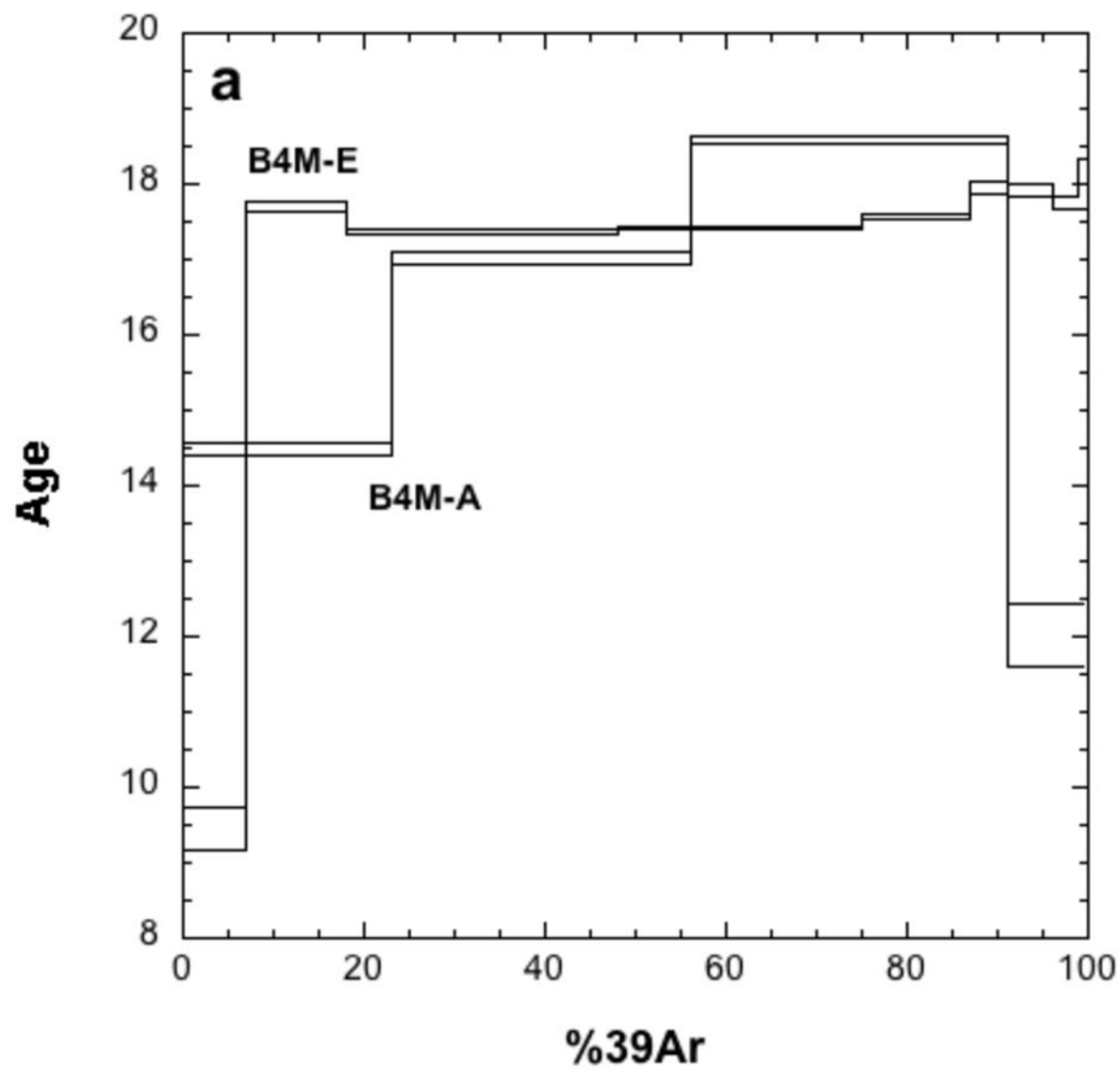
Heri et al. Fig.3d



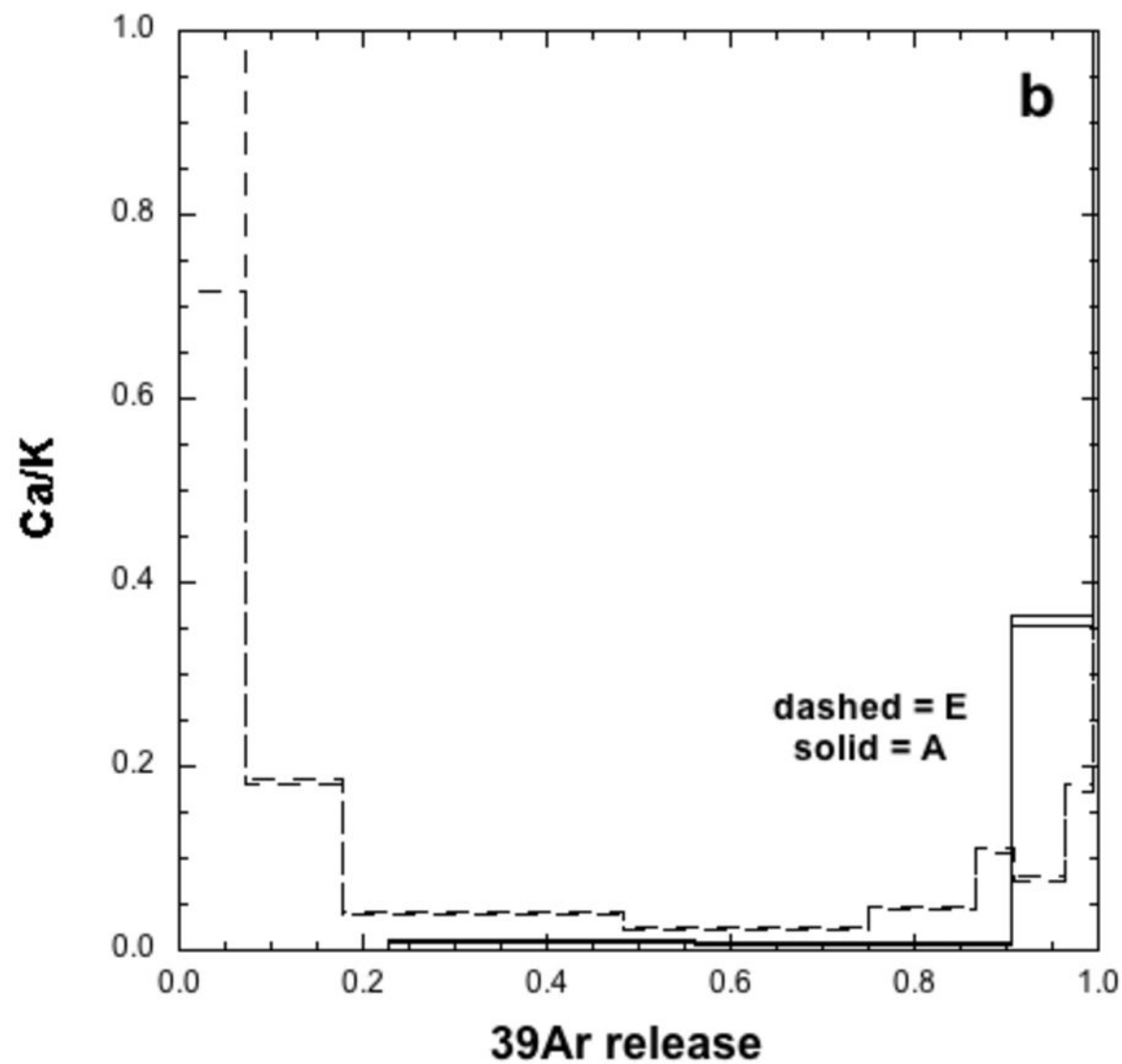
Heri et al. Fig.4



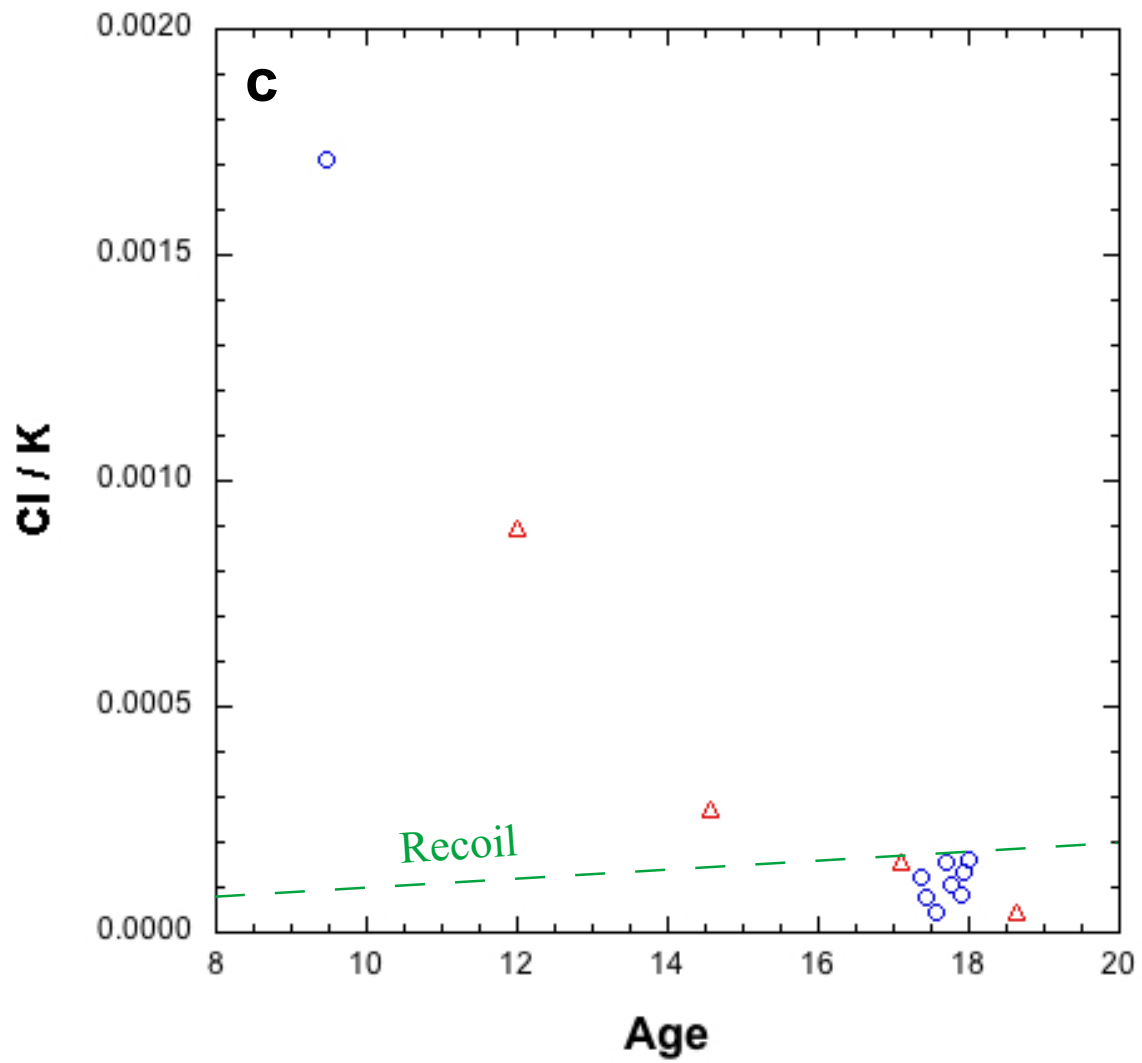
Heri et al. Fig.5a



Heri et al. Fig.5b



Heri et al. Fig.5c



Sample #	Rb ppm	2SE %	Sr ppm	2SE %	$^{87}\text{Rb}/^{86}\text{Sr}$	2SE abs.	$^{87}/^{86}\text{Sr}$	2SE abs.
B4M-A (< 0.6 μm)	160.7	0.4	34.2	0.3	13.62	0.07	0.713434	0.000019
B4M-B (0.6-2 μm)	112.7	0.3	25.6	0.3	12.74	0.02	0.713145	0.000020
B4M-C (2-6 μm)	77.9	0.3	18.7	0.3	12.04	0.04	0.713014	0.000020
B4M-D (6-20 μm)	47.2	0.3	10.0	0.3	13.62	0.02	0.716030	0.000040
B4M-E (> 20 μm)	24.9	0.3	2.4	0.3	30.29	0.02	0.719482	0.000041

Heri et al. Tab.1

Cation Total O = 24.0

	Si	Mg	K	F	Fe	Al	Ca	Na	Mn	Ti	Total	Mg/Fe	F/Fe	Mg+Fe	Al+Fe+Mg	F/Mg	Na/Mg
B4M_flat1	6.810	0.233	2.075	0.024	0.250	5.768	0.002	0.117	0.001	0.074	15.353	0.932	0.097	0.483	6.251	0.104	0.500
B4M_flat2	6.759	0.259	2.046	0	0.241	5.820	0	0.116	0.001	0.085	15.327	1.073	0.000	0.500	6.320	0.000	0.449
B4M_flat3	6.705	0.235	2.082	0	0.236	5.909	0	0.119	0.002	0.077	15.364	0.996	0.000	0.471	6.380	0.000	0.504
B4M_flat4	6.846	0.289	2.059	0.047	0.242	5.695	0	0.095	0.002	0.078	15.354	1.195	0.194	0.531	6.226	0.162	0.329
B4M_flat5	6.781	0.235	2.061	0.041	0.230	5.830	0	0.127	0.002	0.066	15.373	1.022	0.180	0.465	6.295	0.176	0.541
B4M_flat7	6.743	0.222	2.086	0	0.249	5.867	0.001	0.127	0.001	0.067	15.363	0.890	0.000	0.471	6.338	0.000	0.575
B4M_flat8	6.727	0.195	2.024	0	0.235	5.948	0.001	0.127	0.001	0.059	15.316	0.831	0.000	0.430	6.378	0.000	0.649
B4M_flat10	6.768	0.241	2.113	0.038	0.238	5.834	0	0.096	0.004	0.064	15.395	1.011	0.161	0.479	6.313	0.159	0.398
B4M_flat11	7.068	0.372	2.047	0.062	0.287	5.354	0	0.091	0.001	0.052	15.334	1.296	0.215	0.659	6.013	0.166	0.245
B4M_flat11b	7.129	0.405	2.030	0.082	0.287	5.263	0	0.066	0.004	0.052	15.318	1.411	0.286	0.692	5.955	0.202	0.164
B4M_flat11c	7.085	0.397	2.050	0.101	0.287	5.309	0	0.098	0.003	0.053	15.383	1.383	0.353	0.684	5.993	0.255	0.247
B4M_flat12	6.753	0.215	2.065	0.038	0.253	5.881	0	0.119	0.002	0.055	15.380	0.849	0.148	0.468	6.349	0.175	0.556
B4M_flat13	6.693	0.178	2.064	0.031	0.221	6.005	0	0.124	0.003	0.055	15.373	0.804	0.139	0.399	6.404	0.173	0.700
B4M_flat14	6.769	0.231	2.076	0.091	0.272	5.813	0	0.133	0.005	0.064	15.455	0.851	0.334	0.503	6.316	0.392	0.575
B4M_flat15	6.752	0.216	2.091	0.090	0.209	5.906	0	0.119	0.002	0.052	15.437	1.035	0.428	0.425	6.331	0.414	0.551
B4M_flat16	6.909	0.305	2.037	0.065	0.279	5.609	0	0.100	0.001	0.058	15.362	1.091	0.234	0.584	6.193	0.214	0.329
B4M_flat17	6.810	0.270	2.081	0.076	0.266	5.746	0	0.117	0.002	0.062	15.430	1.017	0.284	0.536	6.282	0.279	0.433
B4M_flat18	6.758	0.225	2.098	0.047	0.223	5.863	0	0.108	0.003	0.067	15.392	1.008	0.209	0.448	6.311	0.207	0.481
B4M_flat19	7.067	0.404	2.088	0.123	0.280	5.332	0	0.078	0.004	0.048	15.424	1.443	0.439	0.684	6.016	0.304	0.194
B4M_flat20	6.902	0.318	2.040	0.021	0.301	5.588	0	0.109	0.005	0.058	15.342	1.058	0.069	0.619	6.207	0.066	0.342
B4M_flat21	6.812	0.237	2.090	0.009	0.219	5.819	0	0.078	0.001	0.053	15.318	1.083	0.039	0.456	6.275	0.036	0.330
B4M_flat22	6.792	0.208	2.130	0.048	0.227	5.851	0	0.102	0.001	0.045	15.403	0.918	0.212	0.435	6.286	0.231	0.487
B4M_flat23	6.773	0.235	2.058	0.084	0.267	5.828	0	0.136	0.001	0.056	15.438	0.882	0.313	0.502	6.330	0.356	0.576
B4M_flat24	6.820	0.268	2.043	0.057	0.276	5.743	0	0.128	0.003	0.057	15.394	0.971	0.205	0.544	6.287	0.211	0.476
B4M_flat25	7.151	0.416	2.059	0.050	0.305	5.210	0	0.083	0.004	0.044	15.322	1.364	0.163	0.721	5.931	0.119	0.200
B4M_flat26	6.810	0.262	2.097	0.067	0.261	5.755	0	0.123	0.001	0.057	15.432	1.002	0.258	0.523	6.278	0.257	0.469
B4M_flat27	7.084	0.409	2.079	0.107	0.273	5.287	0	0.073	0.004	0.070	15.386	1.498	0.392	0.682	5.969	0.262	0.179
B4M_flat28	6.997	0.342	2.098	0.042	0.271	5.428	0	0.089	0.006	0.076	15.349	1.261	0.155	0.613	6.041	0.123	0.262
B4M_flat29	6.743	0.187	2.039	0.055	0.244	5.914	0	0.119	0.008	0.062	15.372	0.768	0.226	0.431	6.345	0.295	0.637
B4M_flat30	6.835	0.233	2.088	0.102	0.279	5.728	0	0.115	0.003	0.061	15.444	0.834	0.367	0.512	6.240	0.439	0.494
B4M_flat31	6.762	0.166	2.021	0.042	0.237	5.906	0	0.138	0.001	0.067	15.340	0.698	0.175	0.403	6.309	0.251	0.836
B4M_flat32	6.862	0.219	2.057	0.047	0.263	5.703	0	0.126	0.004	0.072	15.352	0.831	0.178	0.482	6.185	0.214	0.574
B4M_flat33	6.713	0.145	2.074	0.047	0.224	5.975	0	0.140	0.002	0.067	15.387	0.646	0.208	0.369	6.344	0.322	0.970
B4M_flat34	6.815	0.207	2.106	0.062	0.239	5.798	0	0.098	0.003	0.061	15.389	0.867	0.261	0.446	6.244	0.301	0.471

B4M_flat35	6.897	0.264	2.111	0.056	0.261	5.640	0	0.102	0.003	0.055	15.388	1.010	0.213	0.525	6.165	0.211	0.387
B4M_flat36	6.792	0.220	2.107	0.012	0.257	5.802	0	0.114	0.005	0.061	15.370	0.855	0.047	0.477	6.279	0.055	0.520
B4M_flat37	6.766	0.183	2.052	0	0.252	5.885	0	0.125	0.003	0.056	15.322	0.727	0.000	0.435	6.320	0.000	0.681
B4M_flat38	6.821	0.209	2.049	0.052	0.263	5.781	0	0.100	0.004	0.068	15.347	0.795	0.197	0.472	6.253	0.247	0.479
B4M_flat39	6.861	0.246	2.084	0	0.265	5.686	0	0.094	0.003	0.073	15.312	0.930	0.000	0.511	6.197	0.000	0.381
B4M_flat40	6.837	0.245	2.091	0.059	0.256	5.708	0	0.107	0.002	0.081	15.386	0.957	0.230	0.501	6.209	0.240	0.438
B4M_flat41	6.852	0.232	2.082	0.030	0.250	5.709	0	0.111	0.002	0.077	15.344	0.927	0.120	0.482	6.191	0.129	0.477
B4M_flat42	6.884	0.233	2.082	0.056	0.264	5.663	0	0.102	0.002	0.073	15.359	0.884	0.210	0.497	6.160	0.238	0.435
B4M_flat43	6.842	0.247	2.094	0.011	0.278	5.693	0	0.098	0.003	0.077	15.341	0.888	0.038	0.525	6.218	0.043	0.395
B4M_flat44	6.798	0.221	2.082	0.105	0.270	5.778	0	0.129	0.003	0.069	15.455	0.818	0.390	0.491	6.269	0.477	0.583
B4M_flat45	6.726	0.169	2.088	0.016	0.240	5.954	0	0.108	0	0.055	15.355	0.703	0.065	0.409	6.363	0.092	0.639
B4M_flat46	6.875	0.233	2.081	0.031	0.267	5.683	0	0.108	0.001	0.065	15.343	0.874	0.116	0.500	6.183	0.133	0.461
B4M_flat47	6.737	0.172	2.095	0.023	0.227	5.928	0	0.117	0	0.064	15.363	0.759	0.099	0.399	6.327	0.131	0.680
B4M_flat48	6.685	0.127	2.079	0.028	0.206	6.076	0	0.105	0	0.046	15.352	0.616	0.133	0.333	6.409	0.217	0.829
B4M_flat49	6.668	0.133	2.087	0.033	0.216	6.083	0	0.102	0.002	0.048	15.371	0.614	0.151	0.349	6.432	0.247	0.766
B4M_flat50	6.836	0.224	2.056	0.055	0.255	5.761	0	0.113	0.002	0.061	15.363	0.878	0.216	0.479	6.240	0.246	0.506
B4M_flat51	6.753	0.192	2.113	0.099	0.225	5.892	0	0.098	0.004	0.065	15.441	0.851	0.439	0.417	6.309	0.515	0.511
B4M_flat52	6.643	0.135	2.086	0.071	0.215	6.103	0	0.094	0.001	0.059	15.406	0.627	0.329	0.350	6.453	0.526	0.696
B4M_flat53	6.719	0.153	2.114	0.019	0.220	5.983	0	0.091	0.002	0.056	15.356	0.693	0.086	0.373	6.356	0.125	0.593
B4M_flat54	7.157	0.325	2.048	0.048	0.304	5.243	0	0.088	0.004	0.061	15.277	1.069	0.158	0.629	5.872	0.148	0.269
B4M_flat55	6.773	0.171	2.089	0.007	0.243	5.872	0	0.137	0.003	0.058	15.353	0.705	0.028	0.414	6.286	0.040	0.802
B4M_flat56	6.988	0.250	2.093	0.067	0.287	5.498	0	0.093	0.004	0.071	15.351	0.870	0.234	0.537	6.035	0.270	0.373
B4M_flat58	6.691	0.188	2.072	0.091	0.220	6.001	0	0.128	0.001	0.053	15.445	0.854	0.413	0.408	6.409	0.484	0.683
B4M_flat59	6.633	0.140	2.084	0	0.194	6.112	0	0.138	0.000	0.061	15.362	0.720	0.000	0.334	6.446	0.000	0.988
B4M_flat60	6.852	0.290	2.064	0.003	0.289	5.670	0	0.118	0.001	0.060	15.347	1.003	0.012	0.579	6.249	0.012	0.406
B4M_flat61	6.751	0.222	2.087	0.024	0.241	5.874	0	0.112	0.005	0.060	15.376	0.921	0.100	0.463	6.337	0.109	0.503
B4M_flat62	6.741	0.164	2.084	0.052	0.196	5.947	0	0.122	0.001	0.066	15.374	0.839	0.263	0.360	6.307	0.313	0.743
B4M_flat63	6.978	0.362	2.049	0.064	0.303	5.441	0	0.109	0.004	0.067	15.378	1.195	0.212	0.665	6.106	0.177	0.302
B4M_flat64	6.884	0.317	2.067	0.051	0.296	5.597	0	0.120	0.003	0.064	15.398	1.069	0.171	0.613	6.210	0.160	0.379
B4M_flat65	6.986	0.347	2.088	0.068	0.295	5.431	0	0.105	0	0.071	15.391	1.177	0.230	0.642	6.073	0.196	0.302
B4M_vert1	6.689	0.176	2.034	0.046	0.226	6.003	0	0.140	0.005	0.062	15.380	0.780	0.204	0.402	6.405	0.262	0.792
B4M_vert2	7.093	0.393	2.041	0.009	0.308	5.282	0	0.082	0.001	0.063	15.273	1.276	0.028	0.701	5.983	0.022	0.210
B4M_vert3	6.818	0.281	2.088	0.063	0.238	5.729	0	0.104	0.001	0.077	15.398	1.179	0.263	0.519	6.248	0.223	0.371
B4M_vert4	6.750	0.217	2.006	0	0.259	5.803	0.106	0.117	0.012	0.070	15.340	0.836	0.000	0.476	6.279	0.000	0.539
B4M_vert5	7.075	0.420	2.075	0.088	0.281	5.303	0	0.064	0.002	0.061	15.370	1.495	0.313	0.701	6.004	0.210	0.152
B4M_vert6	7.206	0.419	1.968	0.109	0.330	5.100	0.015	0.085	0.004	0.071	15.308	1.269	0.329	0.749	5.849	0.260	0.203
B4M_vert7	6.776	0.248	2.071	0.024	0.245	5.819	0.001	0.112	0.000	0.067	15.364	1.013	0.099	0.493	6.312	0.098	0.453
B4M_vert8	7.009	0.380	2.052	0.043	0.280	5.409	0.002	0.084	0.002	0.070	15.330	1.357	0.155	0.660	6.069	0.114	0.220

B4M_vert9	6.879	0.328	2.066	0.097	0.319	5.569	0	0.109	0.001	0.076	15.444	1.029	0.303	0.647	6.216	0.294	0.332
B4M_vert10	6.820	0.257	2.063	0.064	0.259	5.736	0.002	0.095	0.004	0.078	15.377	0.993	0.248	0.516	6.252	0.250	0.368
B4M_vert6b	7.158	0.425	1.991	0.099	0.320	5.168	0.005	0.083	0.005	0.070	15.324	1.328	0.309	0.745	5.913	0.233	0.194
B4M_vert6c	7.126	0.315	1.955	0.062	0.273	5.339	0.009	0.072	0.004	0.063	15.217	1.152	0.229	0.588	5.927	0.198	0.227
B4M_vert6d	7.150	0.382	1.871	0.055	0.298	5.248	0.012	0.097	0.001	0.076	15.189	1.280	0.183	0.680	5.928	0.143	0.255
B4M_vert11	6.813	0.238	2.035	0.025	0.269	5.766	0.001	0.107	0.005	0.070	15.328	0.884	0.091	0.507	6.273	0.103	0.448
B4M_vert12	6.775	0.235	2.052	0.059	0.278	5.798	0	0.128	0.001	0.074	15.400	0.845	0.211	0.513	6.311	0.250	0.545
B4M_vert13	6.894	0.337	2.058	0.014	0.292	5.564	0.001	0.091	0.005	0.078	15.334	1.154	0.047	0.629	6.193	0.041	0.271
B4M_vert14	7.113	0.427	2.063	0.045	0.291	5.238	0	0.084	0.003	0.062	15.326	1.467	0.154	0.718	5.956	0.105	0.198
B4M_vert15	6.744	0.219	2.068	0.048	0.250	5.881	0	0.122	0.002	0.062	15.396	0.875	0.192	0.469	6.350	0.220	0.556
B4M_vert15b	6.686	0.210	2.103	0.055	0.283	5.929	0.001	0.107	0.005	0.065	15.443	0.740	0.195	0.493	6.422	0.264	0.509
B4M_vert16	6.720	0.218	2.038	0.047	0.256	5.903	0	0.117	0.004	0.075	15.377	0.850	0.182	0.474	6.377	0.214	0.537
B4M_vert17	7.100	0.418	2.038	0.066	0.292	5.270	0.004	0.091	0.002	0.057	15.338	1.432	0.225	0.710	5.980	0.157	0.217
B4M_vert18	6.758	0.211	2.071	0.079	0.226	5.872	0.001	0.095	0.002	0.077	15.392	0.935	0.349	0.437	6.309	0.373	0.448
B4M_vert19	6.724	0.193	2.060	0.015	0.227	5.954	0.002	0.125	0.005	0.051	15.357	0.851	0.068	0.420	6.374	0.080	0.649
B4M_vert20	6.709	0.205	2.033	0	0.228	5.965	0.001	0.101	0	0.067	15.309	0.898	0.000	0.433	6.398	0.000	0.495
B4M_vert21	6.792	0.243	1.993	0.038	0.237	5.840	0.003	0.084	0.003	0.066	15.298	1.025	0.160	0.480	6.320	0.156	0.344
B4M_vert22	7.006	0.342	2.083	0.089	0.320	5.392	0	0.098	0.003	0.072	15.406	1.069	0.277	0.662	6.054	0.259	0.288
B4M_vert22b	6.943	0.318	2.081	0.026	0.296	5.504	0	0.094	0.003	0.077	15.341	1.075	0.087	0.614	6.118	0.081	0.294
B4M_vert22c	6.969	0.318	2.099	0.099	0.302	5.451	0	0.094	0.002	0.084	15.417	1.054	0.326	0.620	6.071	0.310	0.294
B4M_vert23	7.038	0.363	2.082	0.028	0.277	5.385	0	0.077	0.006	0.060	15.316	1.310	0.100	0.640	6.025	0.076	0.213
B4M_vert24	6.695	0.183	2.027	0.015	0.232	6.001	0	0.119	0.001	0.059	15.333	0.788	0.066	0.415	6.416	0.084	0.653
B4M_vert25	7.032	0.374	2.077	0.057	0.279	5.382	0	0.095	0.002	0.061	15.358	1.341	0.203	0.653	6.035	0.151	0.255
B4M_vert26	6.719	0.207	2.092	0.029	0.242	5.928	0	0.126	0.003	0.055	15.401	0.857	0.121	0.449	6.377	0.141	0.607
B4M_vert27	7.043	0.384	1.964	0.046	0.303	5.362	0.010	0.094	0.004	0.070	15.279	1.267	0.150	0.687	6.049	0.119	0.244
B4M_vert28	6.872	0.269	2.093	0.045	0.264	5.678	0	0.101	0.004	0.053	15.378	1.019	0.169	0.533	6.211	0.166	0.374
B4M_vert29	6.726	0.234	2.047	0.032	0.260	5.897	0.002	0.115	0.004	0.061	15.378	0.900	0.125	0.494	6.391	0.139	0.490
B4M_vert30	7.040	0.380	2.055	0.082	0.268	5.373	0.001	0.085	0.001	0.071	15.357	1.418	0.307	0.648	6.021	0.217	0.224
B4M_vert31	6.751	0.178	2.011	0.019	0.229	5.932	0.004	0.111	0	0.064	15.299	0.777	0.083	0.407	6.339	0.106	0.626
B4M_vert32	6.972	0.334	1.983	0.047	0.290	5.498	0.001	0.093	0.002	0.072	15.292	1.150	0.161	0.624	6.122	0.140	0.280
B4_vert33	6.753	0.189	2.017	0.047	0.221	5.939	0.004	0.117	0.005	0.051	15.341	0.853	0.210	0.410	6.349	0.247	0.619
B4_vert34	6.949	0.367	2.094	0.054	0.254	5.512	0	0.075	0	0.064	15.369	1.445	0.211	0.621	6.133	0.146	0.205
B4_vert35	7.079	0.412	2.072	0.048	0.280	5.299	0	0.081	0	0.062	15.333	1.471	0.173	0.692	5.991	0.117	0.197
B4_vert36	6.705	0.207	2.054	0	0.217	5.965	0	0.107	0.003	0.068	15.326	0.955	0.000	0.424	6.389	0.000	0.516
B4_vert37	6.695	0.188	2.071	0.048	0.215	5.985	0.002	0.109	0.000	0.069	15.382	0.874	0.223	0.403	6.388	0.255	0.580
B4_vert38	6.781	0.232	2.042	0.013	0.226	5.856	0.003	0.097	0	0.062	15.312	1.028	0.058	0.458	6.314	0.056	0.418
B4_vert39	7.155	0.419	2.065	0.126	0.295	5.197	0.001	0.086	0.004	0.050	15.398	1.420	0.427	0.714	5.911	0.300	0.206
B4_vert40	7.115	0.415	2.066	0.049	0.291	5.256	0.003	0.071	0.004	0.052	15.322	1.426	0.168	0.706	5.962	0.118	0.172
B4_vert41	6.937	0.363	2.076	0.017	0.269	5.515	0.001	0.079	0.004	0.070	15.331	1.349	0.064	0.632	6.147	0.048	0.219

B4_vert42	6.764	0.273	2.094	0.048	0.268	5.783	0.002	0.109	0.005	0.073	15.420	1.019	0.181	0.541	6.324	0.177	0.400
B4_vert43	7.032	0.405	2.044	0.107	0.284	5.370	0	0.084	0.004	0.062	15.392	1.426	0.376	0.689	6.059	0.264	0.208
B4_vert44	6.803	0.249	2.086	0.036	0.246	5.780	0.002	0.099	0.003	0.066	15.370	1.010	0.148	0.495	6.275	0.146	0.399
B4_vert45	6.808	0.258	2.028	0.004	0.251	5.791	0	0.108	0.005	0.058	15.310	1.028	0.014	0.509	6.300	0.014	0.419
B4_vert46	7.165	0.467	1.960	0.104	0.292	5.193	0.007	0.080	0.003	0.045	15.316	1.599	0.356	0.759	5.952	0.223	0.172
B4_vert47	6.652	0.166	2.066	0.010	0.220	6.055	0.001	0.107	0.002	0.069	15.348	0.754	0.046	0.386	6.441	0.062	0.645
B4_vert48	6.656	0.193	2.079	0.073	0.220	6.033	0.001	0.118	0.003	0.062	15.437	0.878	0.330	0.413	6.446	0.376	0.611
B4_vert49	6.704	0.191	2.071	0.040	0.217	5.972	0	0.115	0.003	0.064	15.377	0.880	0.183	0.408	6.380	0.208	0.600
B4_vert50	6.741	0.280	2.065	0.079	0.280	5.815	0	0.127	0.003	0.069	15.459	1.000	0.284	0.560	6.375	0.283	0.453
B4_vert51	6.795	0.285	2.085	0.035	0.283	5.737	0.001	0.094	0.002	0.072	15.389	1.007	0.122	0.568	6.305	0.121	0.330
B4_vert52	6.724	0.259	2.073	0.115	0.265	5.862	0	0.127	0.002	0.067	15.493	0.975	0.435	0.524	6.386	0.446	0.490
B4_vert53	6.789	0.228	2.028	0.027	0.223	5.851	0.004	0.107	0.002	0.061	15.319	1.024	0.121	0.451	6.302	0.118	0.469
B4_vert54	7.113	0.443	2.038	0.091	0.292	5.242	0	0.089	0.002	0.055	15.364	1.517	0.311	0.735	5.977	0.205	0.200
B4_vert55	6.710	0.223	2.064	0.019	0.272	5.913	0.002	0.133	0.002	0.057	15.394	0.818	0.069	0.495	6.408	0.085	0.596
B4_vert56	6.802	0.230	2.055	0.060	0.256	5.792	0.002	0.100	0	0.071	15.369	0.899	0.235	0.486	6.278	0.262	0.435
B4_vert57	6.810	0.281	2.044	0.058	0.277	5.735	0.000	0.121	0.001	0.067	15.395	1.016	0.210	0.558	6.293	0.207	0.431
B4_vert58	7.062	0.397	2.066	0.029	0.312	5.304	0.004	0.096	0.002	0.062	15.334	1.273	0.092	0.709	6.013	0.072	0.240
B4_vert59	6.760	0.269	2.082	0.102	0.268	5.813	0.002	0.109	0	0.064	15.468	1.002	0.380	0.537	6.350	0.379	0.406
B4_vert60	7.091	0.406	2.035	0.084	0.337	5.274	0.002	0.098	0.004	0.045	15.376	1.205	0.250	0.743	6.017	0.208	0.240
B4_vert61	6.875	0.297	2.023	0.052	0.289	5.646	0	0.121	0.006	0.059	15.367	1.026	0.179	0.586	6.232	0.174	0.409
B4_vert62	6.730	0.211	2.054	0.069	0.252	5.908	0.001	0.129	0.004	0.059	15.417	0.839	0.273	0.463	6.371	0.325	0.611
B4_vert63	6.899	0.210	1.935	0	0.221	5.748	0.008	0.115	0	0.058	15.194	0.951	0.000	0.431	6.179	0.000	0.549
B4_vert64	6.773	0.238	2.075	0.074	0.257	5.829	0	0.112	0.005	0.059	15.422	0.925	0.286	0.495	6.324	0.310	0.472
B4_vert65	6.761	0.231	2.071	0.033	0.242	5.864	0	0.107	0.004	0.059	15.371	0.954	0.135	0.473	6.337	0.141	0.463
B4_vert66	6.646	0.178	2.077	0	0.219	6.074	0	0.109	0.002	0.053	15.358	0.811	0.000	0.397	6.471	0.000	0.614
B4_vert67	6.876	0.300	2.056	0.026	0.240	5.658	0	0.104	0.002	0.069	15.331	1.249	0.108	0.540	6.198	0.086	0.347
B4_vert68	6.879	0.296	2.077	0	0.258	5.657	0.001	0.077	0	0.062	15.307	1.147	0.000	0.554	6.211	0.000	0.261
B4_vert69	6.678	0.200	2.090	0	0.213	5.983	0.001	0.114	0	0.077	15.355	0.939	0.000	0.413	6.396	0.000	0.568
B4_vert70	7.133	0.467	2.060	0.092	0.292	5.199	0	0.077	0.002	0.053	15.375	1.599	0.315	0.759	5.958	0.197	0.165
B4_vert71	6.701	0.214	2.072	0.052	0.217	5.944	0	0.116	0.003	0.076	15.396	0.987	0.239	0.431	6.375	0.242	0.543
B4_vert72	6.728	0.222	2.065	0.100	0.213	5.909	0	0.109	0.003	0.077	15.426	1.042	0.468	0.435	6.344	0.449	0.492
B4_vert73	6.637	0.160	2.072	0.012	0.212	6.101	0	0.124	0.002	0.051	15.372	0.753	0.057	0.372	6.473	0.075	0.778
B4_vert74	6.664	0.182	2.088	0	0.207	6.005	0.002	0.122	0	0.084	15.355	0.877	0.000	0.389	6.394	0.000	0.674
B4_vert75	6.887	0.356	2.092	0.024	0.273	5.560	0	0.094	0.006	0.079	15.372	1.305	0.089	0.629	6.189	0.068	0.264
B4_vert76	6.912	0.328	2.077	0.041	0.287	5.558	0	0.091	0.003	0.068	15.366	1.144	0.144	0.615	6.173	0.126	0.276
B4_vert77	6.763	0.237	2.029	0.027	0.247	5.865	0	0.125	0	0.058	15.352	0.960	0.110	0.484	6.349	0.115	0.528
B4_vert78	6.691	0.186	2.034	0	0.239	6.005	0	0.131	0.002	0.050	15.339	0.777	0.000	0.425	6.430	0.000	0.705
B4_vert79	6.811	0.252	2.067	0.069	0.243	5.782	0	0.093	0.003	0.064	15.383	1.036	0.285	0.495	6.277	0.275	0.368
B4_vert80	6.811	0.248	2.071	0.034	0.264	5.760	0	0.104	0.002	0.069	15.363	0.941	0.130	0.512	6.272	0.138	0.420

B4_vert81	6.742	0.178	2.044	0.039	0.231	5.933	0	0.097	0	0.069	15.333	0.769	0.169	0.409	6.342	0.220	0.548
B4_vert82	6.756	0.233	2.042	0.016	0.235	5.877	0.001	0.112	0.005	0.061	15.338	0.990	0.066	0.468	6.345	0.067	0.483
B4_vert83	7.008	0.348	2.083	0.031	0.287	5.433	0.001	0.089	0.005	0.054	15.340	1.212	0.108	0.635	6.068	0.089	0.257
B4_vert84	6.915	0.334	2.085	0.070	0.271	5.551	0.001	0.079	0.007	0.074	15.387	1.231	0.256	0.605	6.156	0.208	0.237
B4_vert85	6.850	0.272	2.024	0.043	0.297	5.663	0.022	0.115	0.006	0.070	15.361	0.914	0.146	0.569	6.232	0.160	0.424
B4_vert86	6.790	0.234	1.973	0.044	0.276	5.827	0.002	0.103	0.001	0.064	15.313	0.849	0.158	0.510	6.337	0.187	0.438
B4_vert87	7.066	0.370	2.046	0.103	0.286	5.351	0	0.093	0.004	0.056	15.376	1.294	0.360	0.656	6.007	0.279	0.251
B4_vert88	6.899	0.303	2.068	0.069	0.272	5.605	0	0.102	0.003	0.065	15.387	1.115	0.254	0.575	6.180	0.228	0.337
B4_vert89	6.882	0.292	2.048	0.012	0.261	5.658	0	0.099	0.004	0.060	15.316	1.118	0.046	0.553	6.211	0.041	0.340
B4_vert90	7.107	0.410	2.029	0.107	0.298	5.269	0	0.087	0.007	0.055	15.370	1.376	0.360	0.708	5.977	0.261	0.213
B4_vert91	6.744	0.220	2.083	0.036	0.243	5.893	0.002	0.126	0.002	0.051	15.400	0.904	0.149	0.463	6.356	0.165	0.573
B4_vert92	7.086	0.409	2.076	0	0.299	5.287	0	0.069	0.003	0.056	15.285	1.368	0.000	0.708	5.995	0.000	0.168

Gneiss Whole Rock

WR_test1	6.749	0.196	1.990	0.014	0.247	5.934	0	0.081	0.004	0.062	15.277	0.794	0.055	0.443	6.377	0.069	0.415
WR_test2	6.790	0.210	2.043	0.026	0.240	5.854	0	0.093	0.003	0.059	15.318	0.875	0.107	0.450	6.304	0.122	0.444
WR_darkP1	6.703	0.140	2.058	0.036	0.206	6.018	0	0.131	0.001	0.064	15.356	0.677	0.176	0.346	6.364	0.259	0.937
WR_brightP1	6.963	0.316	2.047	0.045	0.301	5.472	0	0.104	0.003	0.085	15.336	1.049	0.149	0.617	6.089	0.142	0.330
WR_P1_A	6.786	0.242	2.062	0.111	0.287	5.778	0	0.128	0.003	0.067	15.463	0.844	0.387	0.529	6.307	0.458	0.527
WR_P1_B	6.785	0.258	2.083	0.024	0.296	5.752	0	0.135	0.003	0.068	15.404	0.871	0.082	0.554	6.306	0.095	0.522
WR_P1_C	6.794	0.244	2.091	0.033	0.296	5.750	0	0.129	0.004	0.067	15.408	0.825	0.112	0.540	6.290	0.136	0.528
WR_P1_D	6.662	0.150	2.080	0.009	0.209	6.061	0	0.134	0.001	0.060	15.365	0.716	0.041	0.359	6.420	0.057	0.896
WR_P1_E	6.845	0.240	2.065	0.038	0.244	5.754	0	0.094	0.003	0.057	15.339	0.982	0.155	0.484	6.238	0.158	0.392
WR_P1_F	6.806	0.220	2.085	0.019	0.277	5.790	0.002	0.067	0.003	0.063	15.331	0.792	0.068	0.497	6.287	0.086	0.306
WR_P1_G	6.869	0.253	2.095	0.057	0.270	5.677	0	0.095	0.004	0.062	15.382	0.937	0.211	0.523	6.200	0.225	0.377
WR_P1_H	6.793	0.261	2.071	0.047	0.279	5.755	0	0.128	0.005	0.069	15.408	0.935	0.169	0.540	6.295	0.181	0.491
WR_P1_I	6.859	0.271	2.050	0.003	0.300	5.657	0	0.123	0.004	0.068	15.335	0.903	0.011	0.571	6.228	0.013	0.453
WR_P1_J	6.844	0.264	2.061	0.050	0.293	5.682	0	0.115	0.006	0.070	15.384	0.900	0.170	0.557	6.239	0.189	0.436
WR_darkP2	6.797	0.209	2.070	0.035	0.248	5.811	0	0.128	0.004	0.065	15.366	0.844	0.139	0.457	6.268	0.165	0.609
WR_brightP2	6.836	0.269	2.082	0.038	0.285	5.672	0	0.109	0.006	0.083	15.380	0.945	0.134	0.554	6.226	0.142	0.406
WR_P3_A	6.710	0.200	2.049	0.079	0.255	5.933	0	0.145	0.001	0.064	15.436	0.784	0.309	0.455	6.388	0.395	0.728
WR_P3_B	6.708	0.172	2.048	0	0.213	5.989	0	0.132	0.005	0.061	15.327	0.807	0.000	0.385	6.374	0.000	0.767
WR_P3_C	6.795	0.224	2.045	0.041	0.277	5.793	0	0.131	0.002	0.066	15.373	0.807	0.149	0.501	6.294	0.184	0.586
WR_P3_D	6.772	0.198	2.063	0.043	0.232	5.870	0	0.108	0.003	0.066	15.355	0.853	0.184	0.430	6.300	0.215	0.544
WR_P3_F	6.645	0.165	2.067	0.019	0.226	6.072	0	0.124	0.002	0.057	15.377	0.728	0.084	0.391	6.463	0.116	0.756
WR_P3_G	6.840	0.226	2.077	0.041	0.255	5.744	0	0.101	0.001	0.067	15.352	0.887	0.162	0.481	6.225	0.183	0.446
WR_P3_H	6.633	0.128	2.055	0.019	0.218	6.129	0	0.156	0.003	0.043	15.383	0.586	0.087	0.346	6.475	0.148	1.217
WR_P3_E	6.753	0.188	2.061	0.038	0.239	5.899	0	0.128	0	0.062	15.369	0.788	0.159	0.427	6.326	0.201	0.680

Heri et al. Tab.2

T (°C)	40Ar total	Err. 40Ar	39Ar	Err. 39Ar	% 39Ar	38Ar	Err. 38Ar	38ArCl	37Ar	Err. 37Ar	36Ar	Err. 36Ar	Age	Error age	Ca/K	Error Ca/K	Cl/K	Error Cl/K
E (> 20 μm) m=0.0105 g J=.000475																		
600	7.308E-09	7.3E-11	2.151E-10	1.3E-12	7.1	7.71E-12	5.6E-13	2.07E-12	1.17E-11	3.3E-12	1.668E-11	2.3E-13	9.46	0.30	0.1089	0.0304	0.00171	0.00047
700	1.432E-08	2.7E-12	3.278E-10	2.9E-13	17.8	8.90E-12	2.1E-14	2.89E-13	3.30E-12	4.1E-14	2.543E-11	9.3E-14	17.70	0.07	0.0202	0.0002	0.00016	0.00002
820	2.426E-08	4.3E-12	9.273E-10	9.4E-13	48.3	1.50E-11	3.4E-14	6.38E-13	2.04E-12	4.1E-14	1.822E-11	6.8E-14	17.37	0.03	0.0044	0.0001	0.00012	0.00001
870	2.091E-08	3.3E-12	8.101E-10	7.8E-13	75.0	1.26E-11	4.4E-14	3.58E-13	1.07E-12	4.8E-14	1.474E-11	5.7E-14	17.43	0.02	0.0026	0.0001	0.00008	0.00001
920	1.085E-08	5.8E-12	3.559E-10	3.2E-13	86.7	6.50E-12	1.5E-14	9.15E-14	9.01E-13	3.2E-14	1.191E-11	4.7E-14	17.58	0.04	0.0051	0.0002	0.00005	0.00001
970	5.077E-09	1.7E-12	1.266E-10	1.5E-13	90.8	3.11E-12	7.6E-15	9.61E-14	7.48E-13	1.6E-14	8.164E-12	3.6E-14	17.95	0.07	0.0118	0.0002	0.00014	0.00002
1050	7.361E-09	2.9E-12	1.692E-10	1.8E-13	96.4	4.48E-12	1.1E-14	8.14E-14	7.28E-13	2.4E-14	1.289E-11	5.1E-14	17.91	0.08	0.0086	0.0003	0.00009	0.00002
1183	3.869E-09	3.8E-12	9.101E-11	1.2E-13	99.4	2.37E-12	5.2E-15	5.50E-14	8.79E-13	2.0E-14	6.679E-12	3.2E-14	17.76	0.09	0.0193	0.0004	0.00011	0.00002
1350	1.481E-09	1.1E-12	1.870E-11	3.7E-14	100.0	9.24E-13	4.1E-15	1.71E-14	6.26E-13	2.3E-14	3.676E-12	2.4E-14	17.99	0.33	0.0670	0.0025	0.00016	0.00006
A (< 0.6 μm) m=0.0114 g J=.000475																		
400	2.846E-08	1.2E-12	6.157E-10	9.5E-13	22.9	1.96E-11	4.3E-14	9.42E-13	-2.3E-15	1.4E-14	6.098E-11	2.2E-13	14.48	0.09	-7.5E-06	4.6E-05	0.00027	0.00002
500	3.557E-08	4.1E-11	8.922E-10	1.9E-12	56.2	2.25E-11	8.1E-14	7.90E-13	1.20E-13	1.0E-14	6.013E-11	2.6E-13	17.02	0.08	0.00027	0.00002	0.00016	0.00002
590	3.431E-08	3.3E-11	9.244E-10	1.3E-12	90.6	2.00E-11	3.9E-14	2.16E-13	9.20E-14	4.3E-15	4.788E-11	1.8E-13	18.59	0.06	0.00020	0.00001	0.00004	0.00001
660	1.272E-08	2.1E-10	2.353E-10	3.5E-12	99.4	9.90E-12	2.7E-13	1.18E-12	1.16E-12	1.8E-14	3.186E-11	2.9E-13	12.01	0.41	0.00988	0.00015	0.00089	0.00021
1350	1.117E-08	1.8 e-12	1.679E-11	2.6 e-14	100.0	6.67E-12	1.9E-14	1.51E-13	1.61E-12	1.0E-14	3.384E-11	9.2E-14	58.66	1.88	0.19156	0.00256	0.00160	0.00086

Heri et al. Tab.3

